Chemical characterization of fine particulate matter in Changzhou, China and source apportionment with offline aerosol mass spectrometry

Zhaolian Ye[1,2], Jiashu Liu[1], Aijun Gu[1], Feifei Feng[1],Yuhai Liu[1], Chenglu Bi[1], Jianzhong Xu[3], Ling Li[2], Hui Chen[2], Yanfang Chen[2], Liang Dai[2], Quanfa Zhou[1], Xinlei Ge[2,*]

[1]College of Chemistry and Environmental Engineering, Jiangsu University of Technology, Changzhou 213001, China

[2]Jiangsu Key Laboratory of Atmospheric Environment Monitoring and Pollution Control, Collaborative Innovation Center of Atmospheric Environment and Equipment Technology, School of Environmental Sciences and Engineering, Nanjing University of Information Science and Technology, Nanjing 210044, China

[3]State Key Laboratory of Cryospheric Sciences, Northwest Institute of Eco-Environment and Resources, Chinese Academy of Sciences, Lanzhou 730000, China

*Corresponding author, Email: caxinra@163.com

Phone: +86-25-58731394

Abstract: Knowledge on aerosol chemistry in densely populated regions is critical for effective reduction of air pollution, while such studies have not been conducted in Changzhou, an important manufacturing base and populated city in the Yangtze River Delta (YRD), China. This work, for the first time, performed a thorough chemical characterization on the fine particulate matter ($PM_{2.5}$) samples, collected during July 2015 to April 2016 across four seasons in this city. A suite of analytical techniques were employed to measure the organic carbon (OC), elemental carbon (EC), water-soluble organic carbon (WSOC), water-soluble inorganic ions (WSIIs), trace elements, and polycyclic aromatic hydrocarbons (PAHs) in $PM_{2.5}$; in particular, an Aerodyne soot particle aerosol mass spectrometer (SP-AMS) was deployed to probe the chemical properties of water-soluble organic aerosols (WSOA). The average $PM_{2.5}$ concentrations were found to be 108.3 μg m^{-3}, and all identified species were able to reconstruct ~80% of the $PM_{2.5}$ mass. The WSIIs occupied about half of the $PM_{2.5}$ mass (~52.1%), with

SO_4^{2-}, NO_3^- and NH_4^+ as the major ions. On average, nitrate concentrations dominated over sulfate (mass ratio of 1.21), indicating that traffic emissions were more important than stationary sources. OC and EC correlated well with each other and the highest OC/EC ratio (5.16) occurred in winter, suggesting complex OC sources likely including both secondary and primary ones. Concentrations of eight trace elements (Mn, Zn, Al, B, Cr, Cu, Fe, Pb) can contribute up to ~5.0% of $PM_{2.5}$ during winter. PAHs concentrations were also high in winter (140.25 ng m^{-3}), which were predominated by median/high molecular weight PAHs with 5- and 6-rings. The organic matter including both water-soluble and water-insoluble species occupied ~21.5% $PM_{2.5}$ mass. SP-AMS determined that the WSOA had an average atomic oxygen-to-carbon (O/C), hydrogen-to-carbon (H/C), nitrogen-to-carbon (N/C) and organic matter-to-organic carbon (OM/OC) ratios of 0.54, 1.69, 0.11, and 1.99, respectively. Source apportionment of WSOA further identified two secondary OA (SOA) factors (a less oxidized and a more oxidized oxygenated OA) and two primary OA (POA) factors (a nitrogen enriched hydrocarbon-like traffic OA and a local primary OA likely including species from cooking, coal combustion, etc.). On average, the POA contribution overweighed SOA (55% *vs.* 45%), indicating the important role of local anthropogenic emissions to the aerosol pollution in Changzhou. Our measurement also shows the abundance of organic nitrogen species in WSOA, and the source analyses suggest these species likely associated with traffic emissions, which warrants more investigations on PM samples from other locations.

1. Introduction

Aerosol particles are ubiquitous in the atmosphere and play important roles in air quality, global climate, biogeochemical cycle, and human health, etc (e.g., Heal et al., 2012;Cao et al., 2012;Hu et al., 2015). Aerosol pollution can also influence remote territories via long-range transport. Therefore, atmospheric aerosol has received extensive attentions from the government, public and academia (e.g., Zhang et al., 2007a;Jimenez et al., 2009). Particularly, much attentions have been focused on fine

particles ($PM_{2.5}$, aerodynamic diameters less than 2.5 μm) as they can go deeper into the respiratory system, causing more severe health problems than coarse particles (Anderson et al., 2012). However, the concentrations, sources, chemical compositions and formation mechanisms of $PM_{2.5}$ are complicated and can vary greatly with meteorological conditions, seasons and regional/local topography, etc. $PM_{2.5}$ can contain a variety of species, i.e., organic carbon (OC), elemental carbon (EC), trace elements, inorganic salts, and various organic species such as polycyclic aromatic hydrocarbons (PAHs)(e.g., Wang et al., 2015). In China, haze pollution occurred frequently in recent years, and a large number of studies regarding the chemical characterization of fine particles were carried out in many locations (Wang et al., 2006a), such as Shanghai (e.g., Wang et al., 2016a;Zhao et al., 2015), Beijing (e.g., Sun et al., 2014;Hu et al., 2016;Sun et al., 2016), Nanjing (e.g., Zhang et al., 2016;Ding et al., 2013), Lanzhou (e.g., Fan et al., 2014;Xu et al., 2014), Wuhan (e.g., Huang et al., 2016), and other remote sites (Xu et al., 2015), etc.

Yangtze River Delta (YRD) region, located in Eastern China, is experiencing severe atmospheric pollution along with the rapid economic development. Some studies carried out in the YRD investigated different characteristics of the fine aerosols, including the mass loading, composition, hygroscopicity (e.g., Ye et al., 2011;Ge et al., 2015), size distribution, seasonal variation, source, formation pathway, and their impacts on visibility and climate (e.g., Wang et al., 2012). However, these studies were mostly limited in Nanjing (e.g., Hu et al., 2012;Wang et al., 2016b) and Shanghai (e.g., Fu et al., 2012;Qiao et al., 2015;Wang et al., 2012). Changzhou, situated in the western YRD region, between Shanghai and Nanjing, is also a major city and an important manufacturing base due to its geographical advantage. The city has an area of about 4374 km^2 with a population of 4.45 million. Due to elevated emissions of various pollutants, the number of hazy days increased over the past few years in Changzhou as well. To the best of our knowledge, no work has been published specifically on chemical characteristics and source apportionment of fine particles in Changzhou. Thus, it is scientifically and practically important to investigate the $PM_{2.5}$ characteristics in order to

provide efficient control strategies to reduce the PM pollution for Changzhou.

Among various $PM_{2.5}$ constituents, organic aerosol (OA) is a vital component, accounting for a significant, even dominant fraction of $PM_{2.5}$ in ambient air (Zhang et al., 2007a). Thus elucidation of its composition, properties and sources is essential. Apportionment of OA into different sources correctly is a critical step towards enabling efficient air pollution control strategies. Recently, Aerodyne Aerosol Mass spectrometry (AMS) has been used extensively for quantitatively characterizing ambient OA, and the \wealthy mass spectral data allows a better source analyses of OA (Canagaratna et al., 2007). Particularly, positive matrix factorization (PMF), as a standard multivariate factor analysis method, has been widely applied on AMS datasets to distinguish and quantify the OA sources (Zhang et al., 2011). Many previous studies (e.g., Ge et al., 2012a;Ng et al., 2011) have deployed the AMS for online field measurements since AMS can provide real-time information on mass concentrations and size distributions of aerosol particles with very fine time resolution (several seconds to minutes). However, up to now, AMS was typically used for online measurements and only a few studies made efforts to apply it on offline filter sample analyses and source apportionment (Ge et al., 2014;Daellenbach et al., 2016;Sun et al., 2011a;Bozzetti et al., 2017;Mihara and Mochida, 2011;Huang et al., 2014;Xu et al., 2015).

In this study, for the first time, we systematically investigated the chemical characteristics of ambient $PM_{2.5}$ collected in Changzhou nearly across one-year period, providing an overview about the concentrations of $PM_{2.5}$, water-soluble inorganic ions (WSIIs), trace elements, carbonaceous species, water-soluble organic carbon (WSOC), and PAHs, and the relationships among these components. Seasonal variations of different $PM_{2.5}$ components were also discussed. Furthermore, we employed an Aerodyne soot particle aerosol mass spectrometer (SP-AMS) (Onasch et al., 2012;Lee et al., 2015;Wang et al., 2016c) to investigate the properties and potential sources of OA on the basis of high resolution mass spectra determined by the SP-AMS. Findings from this study also add knowledge to the framework of Pan-Eurasian Experiment (PEEX) (Kulmala et al., 2015).

2. Experiments

2.1. Sampling site and $PM_{2.5}$ collection

The sampling site was set on the rooftop of a nine-story building inside the campus of Jiangsu University of Technology in Changzhou (31.7°N, 119.9°E), as shown in Fig. 1. This site locates in the southwestern part of Changzhou, surrounded by a residential area, approximately 0.5 km away from an urban street - Zhongwu Road, and has no direct influences from industrial emissions (14.7 km away from the closest industrial plant – Bao Steel). Meteorological parameters including temperature, relative humidity (RH), wind speed (WS), wind direction (WD), and concentrations of gas-phase species such as SO_2 and NO_2 are recorded by the air quality monitoring station inside the campus, which is about 500 meters away from the site. The average meteorological parameters of four seasons are shown in Table 1. The wind rose plots of different seasons are shown in Fig. S1 in the supplement. The wind speed was generally low in Changzhou (on average, 1.1, 1.6, 0.9 and 0.9 m s^{-1} in spring, summer, fall and winter, respectively).

$PM_{2.5}$ were collected onto 90 mm quartz fiber filters (Whatman, QM-A) using a medium volume sampler (TH-150 C, Wuhan Tianhong Ltd., China) with a flow rate of 100 L min^{-1}. The filters, wrapped in aluminum foil, were prebaked at 450 °C for 4 hours prior to sampling. The sampler began to collect particles at 9:00 am and stopped at 5:00 am of the following day, ensuring the duration time for each sample of 20 hours. A total of 69 $PM_{2.5}$ samples were collected: 20 July - 19 August 2015 (summer, 11 samples), 18 September - 25 October 2015 (fall, 23 samples), 7 December 2015 - 15 January 2016 (winter, 24 samples) and 1 March - 12 April 2016 (spring, 11 samples).

Before and after sampling, the filters were conditioned under constant temperature (22±1°C) and relative humidity (45±5%) for 48 h and weighted by a microbalance (precision of 0.01 mg). The filters were then wrapped and sealed in aluminum foil envelopes separately, stored in a freezer at −20 °C until. Note filter-based measurements are inevitably subjected to various sampling artifacts including evaporation of semi-volatile species, and absorption of gases. Nitrate in the form of ammonium nitrate may have some evaporation loss as it is sensitive to temperature variations during

147 sampling, and absorption of gases may influence the quantification of particle-bound
148 polycyclic aromatic hydrocarbons (PAHs).
149
150 **2.2 Chemical analysis**
151 **2.2.1 IC analysis**
152 One quarter of a filter was put into a glass tube and 25 mL deionized water (18.2
153 MΩ cm^{-1}) was then added. After 15 min ultrasonic extraction, the solution was filtrated
154 through an acetate-cellulose filter with 0.45 μm pore size. Concentrations of the WSIIs
155 in the aqueous extract, including five anions (F^-, Cl^-, NO_2^-, NO_3^-, SO_4^{2-}) and five
156 cations (Na^+, NH_4^+, K^+, Mg^{2+}, Ca^{2+}), were then measured by the ion chromatograph (IC,
157 Dionex ICS-600 for anions and ICS-1500 for cations). The method detection limits
158 (MDLs) were determined to be 18.0, 7.3, 5.2, 6.3, 11.0, 18.7, 3.3, 4.6, 2.6, and 11.5 μg
159 L^{-1} for F^-, Cl^-, NO_2^-, NO_3^-, SO_4^{2-}, Na^+, NH_4^+, K^+, Mg^{2+} and Ca^{2+}, respectively, and all
160 measured concentrations were above the MDLs. Note the filter blanks were treated in
161 the same way, and all data for the samples reported here were blank corrected, other
162 analyses in the following sections were also blank corrected unless specified. The
163 concentrations of all measured species in $PM_{2.5}$ sample were also converted to μg m^{-3}
164 based on the measured concentrations and the air volume pulled through the filter. The
165 uncertainty of the IC measurements, calculated as three times the standard deviation of
166 replicate measurements of blank filters, is shown in Table 2.
167
168 **2.2.2 ICP-OES analysis**
169 Another quarter of a filter was cut and placed in a Teflon vessel, digested with 10
170 mL mixture of HNO_3-HCl (1:1, v:v) in a microwave system (XT-9900A, Shanghai
171 Xintuo Co.) for 45 minutes. After the digested solution cooled down to room
172 temperature, it was filtered through a 0.45 μm acetate-cellulose filter. The filtrate was
173 then diluted using deionized water to 50 mL, and analyzed using Optima 8000 (Perkin
174 Elmer, USA) inductively coupled plasma optical emission spectrometry (ICP-OES) to
175 determine concentrations of eight trace elements (Mn, Zn, Al, B, Cr, Cu, Fe, Pb). It is

worth to mention that we also tried to measure the concentrations of other trace elements such as Ti, Ni, Ba, but found they were mostly below the detection limits thus were not included in this work. All samples were determined in a triplicate, and a difference within 5% was considered acceptable. Measurement uncertainties for trace metals were in the range of 10.3 – 18.5%, with an average of 16.3% (Table 2).

2.2.3 OC/EC and WSOC analysis

Analysis procedure of OC/EC was similar to a previous study (Zhao et al., 2015) . Briefly, OC and EC were measured by the DRI model 2001 thermal/optical carbon analyzer (Atmoslytic Inc. Calabasas, CA) using a 0.526 cm^2 filter punch for each sample, following the IMPROVE TOR protocol (Chow et al., 2004). Filter was measured stepwise at temperatures of 140 °C (OC_1), 280 °C (OC_2), 480 °C (OC_3), and 580 °C (OC_4) under a helium atmosphere, and 580 °C (EC_1), 740 °C (EC_2), and 840 °C (EC_3) under a 2% oxygen/98% helium atmosphere. OC is calculated as $OC_1 + OC_2 + OC_3 + OC_4 + OP$ and EC as $EC_1 + EC_2 + EC_3 - OP$, where OP is the optical pyrolyzed OC. The detection limit of OC was estimated to be 30-80 ng m^{-3} and EC was ~30 ng m^{-3} based on a previous study (Mirante et al., 2014).

The WSOC concentrations were determined by a TOC analyzer (TOC-L, Shimazu, Japan) using a thermos-catalytic oxidation approach. Instrument details and procedure of the WSOC analysis can be found in our previous work (Ge et al., 2014). The MDL was 5.0 μg L^{-1} and measurement uncertainties ranged from 3.4 - 6.0%.

2.2.4 GC-MS analysis for particulate PAHs

Due to the limitation of samples, we only analyzed PAHs for spring and winter samples. The analysis was conducted following the standard procedure, similar to the work of Szabó et al. (2015). One quarter of a filter was treated by Soxhelt extraction for 18 hours using 250 mL mixture of *n*-hexane/ethylether (5:1, v/v). To determine the recovery rates, 100 ng of deuterated surrogate standard solution containing naphthalene-d_8 and perylene-d_{12} (o2si, USA) was added into the sample prior to

extraction, and the average recovery rates of d_8 and d_{12} were over 90%. The extracts were then concentrated to about 2 mL by a rotary evaporator, purified in a chromatography column (filled with 3 cm deactivated Al_2O_3, 10g silica gel, 2 cm deactivated Na_2SO_4). The column was first eluted with 25 mL *n*-hexane and the eluate was discarded, then elution was carried out using 30 mL dichloromethane/*n*-hexane (1:1,v:v). Samples containing PAHs were again concentrated to about 2 mL by the rotary evaporation. Finally they were condensed to exactly 1 mL under a gentle N_2 steam in a 60 °C water bath. The extracts are transferred into ampoule bottles and stored in a refrigerator until analysis.

The PAH compounds in the final extracts were analyzed with a gas chromatography - mass spectrometer (GC-MS) (Agilent 7890-7000B, USA), using a DB-5ms capillary column (30 m×0.25 mm×0.5 μm). The instrument conditions were set as follows: injector at 200 °C; ion source at 230 °C; the column was programmed at 40 °C for 2 min, then increased to 100 °C at a rate of 10 °C min^{-1}, held for 1 min, then increased to 250 °C at 20 °C min^{-1}, and finally held for 3 min at 250 °C. The mass selective detector was operated in the electron impact mode using 70 eV. Multi reaction monitor modes were employed for the identification and quantification of PAHs.

Before sample analysis, calibration standards at a series of concentrations were prepared from aromatic hydrocarbon standard (O2si, USA) containing 18 PAH compounds (1000 mg L^{-1}), which are naphthalene (NaP) ($C_{10}H_8$), acenaphthylene (Acy) ($C_{12}H_8$), acenaphthene (Ace) ($C_{12}H_{10}$), fluorene (Flu) ($C_{13}H_{10}$), phenanthrene (Phe) ($C_{14}H_{10}$), anthracene (Ant) ($C_{14}H_{10}$), fluoranthene (Flua) ($C_{16}H_{10}$), pyrene (Pyr) ($C_{16}H_{10}$), benzo(a)anthracene (BaA) ($C_{18}H_{12}$), chrysene (Chr) ($C_{18}H_{12}$), benzo(b)fluoranthene (BbF) ($C_{20}H_{12}$), benzo(k)fluoranthene (BkF) ($C_{20}H_{12}$), benzo(a)pyrene(BaP) ($C_{20}H_{12}$), Benzo(e)pyrene (BeP) ($C_{20}H_{12}$), benzo(j)fluoranthene (BjF) ($C_{20}H_{12}$), benzoperylene (BghiP) ($C_{22}H_{12}$), indeno(1,2,3-cd)pyrene ($C_{22}H_{12}$), and dibenz(a,h)anthracene ($C_{22}H_{14}$). These PAHs can be classified by the number of aromatic rings and molecular weights: low molecular weight (LMW) PAHs containing 2- and 3-rings (NaP, Acy, Ace, Flu, Phe, Ant), medium molecular weight (MMW) PAHs containing 4-rings (Flua, Pyr, BaA, Chr)

and high molecular weight (HMW) PAHs containing 5- and 6-rings (BbF, BkF, BjF, BaP, BeP, InP, DBA, BghiP) (Wang et al., 2015;Kong et al., 2015). The calibration was conducted twice prior to analysis. Identification and quantification of each PAH is based on its retention time and peak areas in the calibration curve and sample curve, and the total PAH concentration (ΣPAH) was calculated as the sum of concentrations of all 18 individual PAHs. Figure S2 shows examples of the GC-MS spectra of a few 18-PAHs standards and two surrogate standards (d_8 and d_{12}).

2.2.5 Offline SP-AMS analysis

The Aerodyne AMS is specially designed for online and real-time measurements of the submicron aerosol particles. The instrument has a very fine time resolution thus is powerful in capturing the quick atmospheric processes occurred in real atmosphere. While in this study, we used the SP-AMS for offline filter sample analyses. Compared with the online measurements, there are a few advantages: 1) it can greatly expand the application of AMS because it is often unrealistic to deploy the AMS for very long periods as it requires highly skilled personal to carefully maintain and operate the instrument; 2) for some sites, it is not accessible or not suitable for AMS deployment; 3) AMS analysis of organics can provide more details, for instance the elemental composition, oxidation states, etc., thus can offer useful insights into the origin of OA; 4) offline analyses may introduce artifacts compared with the online measurements, but on the other hand, it also expands the size range as online measurements were often limited in submicron meter range.

The SP-AMS analysis procedure for offline filters was similar to that of Xu et al. (2013). Briefly, for each sample, 1/4 filter was extracted in 25 mL deionized water. The liquid extracts were aerosolized using an atomizer (TSI, Model 3076), and the mist passed through a silica-gel diffusion dryer, leaving dry particles which were subsequently analyzed by the SP-AMS. Note the SP-AMS was operated with the laser off so similar to other AMS measurements; it measured non-refractory organic species that can vaporize fast at the oven temperature of 600 ^{o}C. The instrument employs the 70

eV electron impact (EI) ion generation scheme, all vaporized species were broken into ion fragments with specific mass-to-charge (*m/z*) ratios, and the time-of-flight mass spectrometer outputs the mass spectrum that records the ions according to their signal intensities at different *m/z* ratios. Ion fragments with *m/z* up to 300 amu were recorded in this study. The SP-AMS mass spectra can well represent the total OA constituents, and the bulk OA properties such as elemental ratios including oxygen-to-carbon (O/C), hydrogen-to-carbon (H/C) and nitrogen-to-carbon (N/C) ratios, and the organic mass-to-organic carbon (OM/OC) ratio can be obtained. Note although the SP-AMS is limited in molecular-level speciation analysis (Drewnick, 2012), some compounds can be identified via recognition of their corresponding fingerprint ions, and particular sources can be separated and quantified via further factor analyses.

The SP-AMS data were processed using the Igor-based software toolkit SQUIRREL (version 1.56D) and PIKA (version 1.15D) (downloaded from: http://cires.colorado.edu/jimenez-group/ToFAMSResources/ToFSoftware/index.html), and the analysis procedure was similar to our previous work (Ge et al., 2012b). We did some minor modifications on the fragment table. For example, we set the organic CO_2^+ signal equal to organic CO^+, same as Aiken et al. (2008), as the CO_2^+ signal in $PM_{2.5}$ may come from carbonate not organics, and since we used Argon as carrier gas so different from ambient measurements, the CO^+ signal can be well separated and quantified from N_2^+ at *m/z* 28 (example shown in Fig. S3). Note the scatter plot of original CO_2^+ *vs.* CO^+ signals yielded a slope of 2.24. A recent AMS study using argon as carrier gas on PM_1 filter samples also showed systematically higher CO_2^+ signal than CO^+ but much less than the factor of 2.24, indicating that CO_2^+ signal from $PM_{2.5}$ sample was influenced by CO_2^+ from carbonate. Accordingly, organic H_2O^+, HO^+, O^+ were scaled to CO_2^+ using the ratios proposed by Aiken et al. (2008), and the elemental compositions and H/C, N/C, O/C and OM/OC ratios of OA reported in this study were determined according to the method of Canagaratna et al. (2015).

2.3 Determination of WSOA, WIOA

Mass concentrations of WSOA were calculated by multiplying the WSOC concentrations determined from the TOC analyzer with the OM/OC ratios calculated from the SP-AMS mass spectra (Fig. 2) (equation 1). As shown in Fig. 2, most OM/OC values were within the range of 1.5-2.3, in consistent with the typical OM/OC ratios observed at other urban sites. However, the O/C and OM/OC ratios have no significant seasonal differences, indicating that the WSOA sources were likely similar.

The water-insoluble organic carbon (WIOC) mass was calculated as the difference between the OC determined by the OC/EC analyzer and the WSOC, and a factor of 1.3 suggested by Sun et al. (2011a), was used to convert the WIOC mass to the mass of water-insoluble organic aerosol (WIOA) (equation 2). The total organic aerosol (OA) was treated as the sum of WSOA and WIOA (equation 3).

$$\mathrm{WSOA} = \mathrm{WSOC} \times OM/OC_{WSOA} \quad (1)$$

$$\mathrm{WIOA} = (\mathrm{OC} - \mathrm{WSOC}) * 1.3 \quad (2)$$

$$\mathrm{OA} = \mathrm{WSOA} + \mathrm{WIOA} \quad (3)$$

The measurement uncertainty of WSOA was calculated as the sum of squares of uncertainties of OM/OC ratios and WSOC, ranging from 6.9 - 8.5% (Table 2).

2.4 Source apportionment of WSOA

In this work, we used the PMF Evaluation Toolkit v 2.06 (Ulbrich et al., 2009) and followed the protocol described by Zhang et al. (2011) to conduct the PMF analyses. Typically, inclusion of more samples can provide better PMF results and more scientifically sound interpretation of the sources. But applications of PMF model on a limited number of samples (much less than 100) were also reported previously (e.g., Huang et al., 2014;Sun et al., 2011a), and proven to be able to provide very valuable insights into the sources of OA.

Prior to PMF execution, the following steps were performed: Data and error matrix for WSOA were first adjusted based on equation 1; ions with low signal-to-noise (S/N < 0.2) were removed, and ions with S/N ratios between 0.2 and 2 were downweighted by a factor of 2; Two runs with huge mass loading spikes were removed; all isotopic ions

were removed since their signals are not measured directly but scaled to their parent ions. The PMF solutions were explored by varying the factors from 1 to 8 and the rotational forcing parameter (*f*peak) from −1 to 1 with an increment of 0.1. The four-factor solution with *f*peak=0 was chosen as the best solution. The mass spectra of three-factor and five-factor solutions were presented in Fig. S4. The three-factor solution does not resolve well the oxygenated OA factors as many oxygenated ions were mixed with the primary OA factors. The five-factor solution splits a primary OA factor into two factors with very similar mass profiles. Also, by investigating the correlations of the factors with their corresponding tracer ions, and sulfate, nitrate, etc., of the 3-, 4-, and 5-factor solutions, the 4-factor solution was found to be the most reliable and representative solution.

3. Results and discussion

3.1 Overview of $PM_{2.5}$ concentrations and components

The annual and seasonal average concentrations of $PM_{2.5}$, OC, EC, OA, WSIIs, trace elements and PAHs are summarized in Table 3. As shown in Table 3, the $PM_{2.5}$ concentrations (in μg m^{-3}) were on average (±1σ) 106.0 (±24.4), 80.9 (±37.7), 103.3 (±28.2), and 126.9 (±50.4) in spring, summer, fall and winter, respectively, with annual average of 108.3 (±40.8), comparable to the $PM_{2.5}$ concentrations in Nanjing (106 μg m^{-3} in 2011) (Shen et al., 2014), Tianjin (109.8 μg m^{-3} in 2008) (Gu et al., 2010) and Hangzhou (108.2 μg m^{-3} in 2004-2005) (Liu et al., 2015), but lower than that in Jinan (169 μg m^{-3} in 2010) (Gu et al., 2014). The $PM_{2.5}$ concentrations were highest in winter and relatively low in summer, similar to those found in most cities, such as Tianjin (Gu et al., 2010) and Hangzhou (Liu et al., 2015). Previous studies showed that low concentrations occurring in summer were mainly due to the relatively high boundary layer height, low RH and high temperature (Cheng et al., 2015;Huang et al., 2010). The temperatures and RH values were on average 32.1 ^{o}C and 61.1% in summer during the observation period (Table 1). Overall, the daily average concentration of $PM_{2.5}$ during sampling period exceeds 75 μg m^{-3} - the second-grade national air quality standard

(NAAQS)(GB 3095-2012), and on some heavily polluted days, the $PM_{2.5}$ mass loadings can even exceed 3 times the NAAQS standard.

Overall, the reconstructed $PM_{2.5}$ mass estimated by the sum of OA, EC and WSIIs *vs.* gravimetrically determined $PM_{2.5}$ mass were shown in Fig. 3(a-d). The mass proportions of all measured components to the $PM_{2.5}$ mass are illustrated by five inserted pie charts representing four seasons and the whole year, respectively. On average, the quantified species can occupy 78.6% of the $PM_{2.5}$ mass (note trace elements and PAHs were not included as they were only determined for partial samples), and the mass closure appears to be better for spring and winter samples. Overall, our results are similar to some previous results, such as in Beijing (68%) (Zhang et al., 2013). Details and characteristics of individual components are discussed in the following sections.

3.2 Water soluble inorganic ions

The average concentrations (±σ) of total WSIIs were 66.5 (±17.2), 35.0 (±20.2), 51.0 (±17.2), and 66.8 (±23.6) μg m^{-3} in spring, summer, fall and winter, respectively, with an annual average of 56.4 (±22.9) μg m^{-3}. The level was lowest in summer likely due to the conditions favorable for pollutants dispersion and the wet scavenging of these ions under summer monsoon circulation and precipitation. In total, all WSIIs can account for 62.7%, 43.2%, 49.3% and 52.6% of $PM_{2.5}$ in spring, summer, fall and winter, respectively, with the annual average WSIIs/$PM_{2.5}$ percentage of 52.1%, a little higher than the previously reported value of 45.3% in Handan in 2013 (Meng et al., 2016).

The mass fractions of individual ions to total WSIIs followed the order: NO_3^- (34.2%) > SO_4^{2-} (31.0%) > NH_4^+ (21.2%) > Cl^- (6.0%) > Na^+ (3.8%) > K^+ (1.8%) > Ca^{2+} (1.2%) > Mg^{2+} (0.3%) > NO_2^- and F^- (0.2%) (Fig. 4b). Secondary inorganic ions including SO_4^{2-}, NO_3^-, and NH_4^+, constitute the majority of WSIIs (86.4%) (Fig. 4b) with the highest one being NO_3^-. Nitrate and ammonium concentrations displayed distinct seasonal variations - highest in spring (NO_3^-: 26.4 μg m^{-3}, NH_4^+: 14.8 μg m^{-3}), following by winter (24.1 and 13.1 μg m^{-3}), and lowest in summer (6.8 and 8.2 μg m^{-3}). On the other hand, as a non-volatile species, sulfate concentrations showed no obvious

seasonal differences.

The cross-correlation relationships between different ions can be used to infer their possible common sources. Figure 5 shows the Pearson's correlation coefficients (r) between ions for four seasons, respectively. As illustrated, NH_4^+ had good correlations with SO_4^{2-} and NO_3^- ($r > 0.70$), and particularly high r values were found in winter (with SO_4^{2-}: $r = 0.90$, with NO_3^-: $r = 0.96$) and summer (with SO_4^{2-}: $r = 0.98$, with NO_3^-: $r = 0.93$), indicating these three ions were mainly present in the form of ammonium nitrate and ammonium sulfate. Moreover, the correlations between Na^+ and Cl^- varied largely with the seasons, poor in summer ($r = -0.19$) and winter ($r = 0.37$), indicating different sources for them. For chloride, the annual average Cl^-/Na^+ mass ratio was 1.58, larger than 1.17 in seawater (Zhang et al., 2013), indicating the important contributions from anthropogenic activities to chloride (such as coal combustion) in Changzhou, in particular in winter as the content of Cl^- in winter was significantly elevated. By contrast, K^+ and Cl^- have good correlations (r of 0.86, 0.76, 0.80 and 0.62 in spring, summer, fall and winter), suggesting that K^+ may co-emit with chloride. According to correlation analysis in Fig. 5, Mg^{2+} and Ca^{2+} had good relations with r of 0.58, 0.80, 0.81 and 0.78 in spring, summer, fall and winter, respectively, indicating a similar source likely crustal material for these two ions.

Acidity of $PM_{2.5}$ can be evaluated by AE (anion equivalence) *vs.* CE (cation equivalence), which is calculated by converting the concentrations of anions and cations ($\mu g\ m^{-3}$) into molar concentrations ($\mu mol\ m^{-3}$) using the following equations.

$$\mathrm{AE} = \frac{SO_4^{2-}}{48} + \frac{NO_3^-}{62} + \frac{NO_2^-}{46} + \frac{Cl^-}{35.5} + \frac{F^-}{19} \quad (4)$$

$$\mathrm{CE} = \frac{NH_4^+}{18} + \frac{Mg^{2+}}{12.2} + \frac{Ca^{2+}}{20} + \frac{K^+}{39} + \frac{Na^+}{23} \quad (5)$$

Figure 6a illustrates the scatter plots of CE *vs.* AE in four seasons. The slopes were 1.18, 1.09, 1.03 and 0.93 in spring, summer, fall and winter, respectively, indicating the particles are generally neutralized. Normally, the ratio of $NH_4^+{}_{meas}/\ NH_4^+{}_{pred}$, proposed by Zhang et al. (2007b), can be used to evaluate the existing form of NH_4^+ ion. The predicted NH_4^+ ($NH_4^+{}_{pred}$) was calculated using Equation 6.

$$NH_{4\ pred}^{+} = 18 \times (2 \times \frac{SO_4^{2-}}{96} + \frac{NO_3^-}{62} + \frac{Cl^-}{35.5}) \quad (6)$$

Figure S5 illustrated the ratio of $NH_{4meas}^{+}/NH_{4\ pred}^{+}$ in $PM_{2.5}$ during four seasons. As presented, the ratios were 0.95, 0.93, 0.87, 0.75 in spring, summer, fall and winter, respectively, again verifying that $(NH_4)_2SO_4$ and NH_4NO_3, NH_4Cl were dominant forms for these ionic species.

In addition, the mass ratio of NO_3^- to SO_4^{2-} (NO_3^-/SO_4^{2-}) can be used to determine whether mobile sources (vehicle) or stationary sources (coal combustion) are dominant for these ions (Wang et al., 2006b;Arimoto et al., 1996). When the NO_3^-/SO_4^{2-} mass ratio exceeds 1, it means that particle sources at the observation site are likely dominated by mobile sources, while fixed sources play major roles when the ratio is below 1. In this study, the mass ratios of NO_3^-/SO_4^{2-} were 1.52, 0.43, 0.99 and 1.29 in the spring, summer, fall and winter, respectively, with an annual average ratio of 1.21 (Fig. 6b). The NO_3^-/SO_4^{2-} ratio varied largely with seasons. Note in summer, a lower NO_3^-/SO_4^{2-} ratio may be also ascribed to high temperature which leads to the evaporation of NH_4NO_3, yet the high NO_3^-/SO_4^{2-} in winter and spring is more likely relevant to traffic emissions from Zhongwu Road near the sampling site (Fig. 1).

Previous studies (Xu et al., 2014) have indicated that nitrogen oxidation ratio (NOR = $n NO_3^-/(n NO_3^- + n NO_2)$, n refers to the molar concentration), and sulfur oxidation ratio (SOR = $n SO_4^{2-}/(n SO_4^{2-} + n SO_2)$), can be used to estimate the transformation of NO_2 and SO_2 to particle-phase NO_3^- and SO_4^{2-}. The larger SOR and NOR mean more secondarily formed nitrate and sulfate. The seasonal values for SOR and NOR are plotted in Fig. 6 (c-d). On average, the SOR value appeared to be a bit higher in summer, indicating that strong photochemical oxidation for sulfate formation, while NOR is relatively higher in spring, suggesting conversion of NO_x into nitrate is more efficient in spring in Changzhou.

3.3 Trace elements

Eight trace elements (Mn, Zn, Al, B, Cr, Cu, Fe, Pb) for samples collected during

fall and winter were determined in this study. The average concentrations (μg m^{-3}) are shown in Fig. 7a. The total concentrations were 6.38 μg m^{-3} and 2.77 μg m^{-3}, accounting for 5.0% and 2.7% of the total $PM_{2.5}$ mass during winter and fall, respectively. These values were relatively higher than those in other cities in China, such as 1.74% - 2.04% in Hangzhou (Liu et al., 2015). This probably can be explained by re-suspended dust from building construction around the site during the sampling period. In this study, the observed mean levels of trace elements in fall were in the order of Fe>Zn>B>Al>Cu>Mn>Pb>Cr, and ranked in Zn>Fe>B>Al>Cu>Mn>Pb>Cr during winter (Fig. 7a). In fall , Fe accounted for 39.0% of the total trace metal mass, following by Zn (25.6%), B (12.3%) and Al (9.2%), while in winter Zn contributed the largest (53.7%), following by Fe and B. Overall, Fe and Zn were the two most abundant trace elements in $PM_{2.5}$, accounting for over half of the trace metal mass. Previous work also found that mass loading of Zn was higher than other elements, even higher than Al in Nanjing in 2013 (Qi et al., 2016b;Qi et al., 2016a). Vehicle exhaust is likely one major contributor to the high concentration of Zn.

In general, the correlations between various heavy metals are weak, as depicted in Fig. 7b-d, indicating that the complex sources including both natural and anthropogenic sources for the trace metals observed here. For instance, Cr, Cu, Pb, and Zn can be released from lubricating oils, tail pipe emissions, brake and tire wears (Zhang et al., 2013); Fe and Mg are primarily crustal elements, while Zn and Cu are mainly from anthropogenic sources. Fe and Al were only moderately correlated (for example, in fall with r=0.74, Fig. 7b), showing that they are not from exactly same sources.

3.4 OC and EC

As presented in Table 3, the annual average EC concentration in Changzhou was 5.4 μg m^{-3}, close to Nanjing (5.3 μg m^{-3}) (Li et al., 2015) and Tianjin (5.9 μg m^{-3})(Gu et al., 2010), but lower than those in other cities (e.g., 22.3 μg m^{-3} in Beijing (Duan et al., 2012), and higher than that observed in Shanghai (2.8 μg m^{-3})(Feng et al., 2009). The seasonally averaged OC concentrations were highest in winter (18.3 μg m^{-3}), followed

by fall (13.2 μg m^{-3}) and spring (11.2 μg m^{-3}), and lowest in summer (7.9 μg m^{-3}). The annual average OC concentration was 13.8 μg m^{-3}, comparable to those measured in other cities, such as Shanghai (14.7 μg m^{-3})(Feng et al., 2009), and Tianjin (16.9 μg m^{-3}) (Gu et al., 2010).

The mass concentrations of total carbon (TC, the sum of OC and EC) were 16.0, 12.1, 21.0, 22.3 μg m^{-3} in spring, summer, fall and winter, respectively (Table 2), corresponding mass contributions to $PM_{2.5}$ were 15.0%, 15.0%, 20.3%, and 17.6% with an annual mean of 17.8%. This value was similar to those measured in other cities in China, such as Jinan (10 - 15%)(Gu et al., 2014), Shanghai (15%) (Zhao et al., 2015), and other cities (10 - 15% in Tianjin, Haining, Zhongshan and Deyang; Zhou et al. (2016)). The OA concentrations exhibited similar seasonal variations as $PM_{2.5}$, and ranked in the order: winter (31.2±11.9) > fall (21.6±11.9) > spring (18.9±4.1) > summer (14.0±1.4). The average mass fraction of OA in $PM_{2.5}$ was 21.5%, and the WSOA contributed 77.7% of the total OA mass, similar to the results in Atlanta (approximately 88% in rural Centreville and 77% in urban Atlanta) (Xu et al., 2017).

As illustrated in Fig. 8, the OC/EC ratios varied in different seasons and were largest in winter (5.16) followed by spring (2.38), summer (1.88) and fall (1.75). The largest OC/EC ratio occurred in winter, indicating that secondary organic carbon (SOC) was likely a significant component of $PM_{2.5}$ in winter (Chow et al., 2005), however, the high OC/EC ratio may be influenced by biomass burning and/or coal combustion emissions during wintertime too. A number of previous stuidies about the carbonaceous aerosols in the YRD region also showed that highest OC/EC ratio occurred in winter and the ratio was often larger than 2, such as Shanghai (6.35) (Zhao et al., 2015), Nanjing (2.8)(Li et al., 2015), in consistent with our current results in Changzhou.

3.5 Particulate PAHs analysis with GC-MS and SP-AMS

The average concentrations of the 18 individual PAH and total PAHs (ΣPAHs) in winter and spring are listed in Table 4. It can be seen that InP (% of total PAHs: 12.6 - 14.8%), BghiP (10.8 - 12.3%) and Chr (10.4 - 11.0%) were the three most abundant

PAHs species, followed by BbF (8.69 - 9.39%), BaP (7.37 - 8.29%), BeP (5.83 - 8.61) and BaA (4.53 - 8.27%). The ΣPAHs in $PM_{2.5}$ were found in the range of 14.0 - 365.7 ng m^{-3} (mean: 140.25 ng m^{-3}) and 8.9 - 91.3 ng m^{-3} (mean: 41.42 ng m^{-3}) during winter and spring, respectively. The ΣPAHs concentrations in this study are higher than those reported in Zhenzhou (39 and 111 ng/m^3 in spring and winter)(Wang et al., 2014) and Shanghai (13.7 ng m^{-3} in spring) (Wang et al., 2015), but lower than that reported in Liaoning Province (75 - 1900 ng m^{-3}) (Kong et al., 2010). PAHs with medium (4 rings) and high molecular weights (5 - 6 rings) (MMW and HMW) occupied the majority of PAHs (88.9% in winter and 79.4% in spring). It is well known that MMW and HMW PAHs are usually associated with coal combustion and vehicular emissions (Wang et al., 2015). Prior study in Nanjing (He et al., 2014) also showed the significant contribution of traffic exhaust to some PAHs including BbF, Chr, Flu, InP, BeP, and BghiP, which in total accounted for more than 53% of the total PAHs.

The diagnostic ratios of selected PAHs including Phe/(Ant+Phe), BaP/BghiP, Flua/(Flua+Pyr), BaP/(BaP+Chr) and Phe/(Ant+Phe) can be used to further distinguish the emission sources of PAHs (Szabó et al., 2015). As suggested previously (Feng et al., 2015;Saldarriaga-Noreña et al., 2015), traffic source was characterized with a ratio of BaP/BghiP>0.6, and ratios of Flua/(Flua+Pyr) <0.4, 0.4-0.5, >0.5 suggest sources of petrogenic, fossil fuel combustion and coal/wood combustion, respectively. In this work, the Bap/BghiP of 0.61 (winter) and 0.76 (spring) and Flua/(Flua+Pyr) ratios of 0.47 (winter) and 0.50 (spring), all suggest that local vehicular/fossil fuel combustion emissions could be a prominent contributor to particulate PAHs, and contribution from long-range transport was thus minor. Meanwhile, BaP/(BaP+Chr) ratio of 0.40 (winter) and 0.44 (spring) also point to the source of gasoline emission (Khalili et al., 1995). However, the Phe/(Ant+Phe) ratio of 0.89 (winter) and 0.86 (spring) indicate the coal combustion might be also an important source of PAHs.

On the other hand, by using the SP-AMS, we also identified a series of PAH ions, i.e., $C_{16}H_{10}^+$ (*m/z* 202), $C_{17}H_{12}^+$ (*m/z* 216), $C_{18}H_{10}^+$ (*m/z* 226), $C_{18}H_{12}^+$ (*m/z* 228), $C_{19}H_{12}^+$ (*m/z* 240), $C_{19}H_{14}^+$ (*m/z* 242), $C_{20}H_{10}^+$ (*m/z* 250), $C_{20}H_{12}^+$ (*m/z* 252), $C_{21}H_{12}^+$ (*m/z* 264),

$C_{21}H_{14}^+$ (*m/z* 266), $C_{22}H_{12}^+$ (*m/z* 276), $C_{23}H_{12}^+$ (*m/z* 288), $C_{23}H_{14}^+$ (*m/z* 290), $C_{24}H_{12}^+$ (*m/z* 300), $C_{24}H_{14}^+$ (*m/z* 302), $C_{25}H_{16}^+$ (*m/z* 316), $C_{26}H_{14}^+$ (*m/z* 326), and $C_{26}H_{16}^+$ (*m/z* 328)(Dzepina et al., 2007). Note many PAH ions identified by the SP-AMS were not measured by the GC-MS, and the PAH compound DBA which is determined by the GC-MS was not detected by the SP-AMS. This reflects the different sensitivities and responses to the particle-bound PAHs of these two techniques. Table 5 shows the correlation (*r*) coefficients of the concentrations of a few selected PAHs, and the mass ratios of their concentrations measured by both the GC-MS and SP-AMS (results for SP-AMS were based on measurements of all samples, while results for GC-MS were for 23 samples in winter and spring). It can be seen that the concentrations of GC-MS-determined PAHs correlated very well with each other ($r > 0.92$), while the mass loadings determined by the SP-AMS correlated relatively weak. Also, the mass ratios determined from these two instruments were different. The inconsistencies may be due to the following reasons: (1) SP-AMS broke the parent PAH molecules into fragments due to 70 ev EI, thus concentration of a specific PAH ion from the SP-AMS cannot represent its corresponding parent PAH compound, while GC-MS determined the concentration of molecular PAH compound; (2) One PAH ion in the SP-AMS HRMS may be combination of a few PAHs compounds with the same molecular weights; (3) Sensitivities and responses to the different PAHs of the SP-AMS may be different, thus may lead to uncertainties of the PAHs quantification. Nevertheless, combining GC-MS and SP-AMS to improve the PAH measurements by the SP-AMS is valuable, and will be the subject of our future work.

3.6 Source apportionment of WSOA

3.6.1 WSOA mass spectral profile

To gain further insights into the particulate OA characteristics, we performed the SP-AMS analyses on the water extract of the $PM_{2.5}$ samples, with a focus on OA. The averaged high resolution mass spectra (HRMS) of WSOA classified by six ion categories and five elements are shown in Fig. 9, and the corresponding inset pie charts represent the mass percentages of the ion families and elements, respectively. As

illustrated in Fig. 9a, the $C_xH_y^+$ ion family accounts for 386.2% of the WSOA HRMS, followed by $C_xH_yO^+$ (28.5%), $C_xH_yN_p^+$ (17.7%) and $C_xH_yO_2^+$ (11.2%). It is worth to mention that we found that the $C_xH_yN_p^+$ ions contributed significantly, and the organic N (ON) could occupy 6.4% of the total WSOA mass (Fig.9 b). The average concentration of water-soluble organic nitrogen (WSON) over the sampling period was 1.16 μg N m^{-3} (83.0 nmol N m^{-3}), which is in fact much lower than those measured in Beijing (226 nmol N m^{-3}) (Duan et al., 2009), Qingdao (129 - 199 nmol N m^{-3}) (Shi et al., 2010), Xi,an (300 nmol N m^{-3}) (Ho et al., 2015). The concentration of water-soluble inorganic nitrogen (WSIN, N from ammonium, nitrate and nitrite) was 14.0 μg N m^{-3} base on Table 3, and thus the WSON content corresponds to 7.7% of water-soluble nitrogen (WSN = WSON +WSIN). This values is also much lower than those in Beijing (~30%) (Duan et al., 2009), Qingdao (19 - 22.6%), and Xi,an (22 - 68%) (Ho et al., 2015).

Nevertheless, the level of ON measured here are a few times higher than those observed in other locations from AMS measurements (typically 1 - 3%) (Xu et al., 2014), likely due to the following reasons: First, previous studies were online measurements on non-refractory submicron aerosols, while it is likely that the supermicron fine particles (1-2.5 μm) contain significant nitrogen-containing species, as observed before for marine aerosols (Violaki and Mihalopoulos, 2010). Secondly, we measured only the water-soluble fraction of OA, which may concentrate more nitrogen-containing species (partially from aqueous-phase processing). Thirdly, a recent study reveals that fossil fuel combustion-related emission can be a dominant source of ammonia in urban area (Pan et al., 2016), it thus can act as a significant contributor to amines as amines are often co-emitted with ammonia (Ge et al., 2011b); these amines can be neutralized by inorganic or organic acids and since aminium salts are highly hygroscopic (Ge et al., 2011a), they might be enriched in the WSOA, and generated significant $C_xH_yN_p^+$ ions. Nevertheless, more AMS analyses on the water-extracted $PM_{2.5}$ samples collected from other locations should be conducted to further verify the abundance of ON species in the AMS mass spectra of WSOA.

Overall, the average elemental ratios of the WSOA are 0.54 for O/C, 1.69 for H/C,

583 0.11 for N/C and 1.99 for OM/OC (Fig. 9a). WSOA is on average comprised of 50.2% C，
584 7.,1 % H, 36.1% O, 6.4% N and a negligible fraction (0.2%) of S (Fig. 9b).
585
586 **3.6.2 WSOA sources from PMF analysis**
587 The PMF analysis of the WSOA HRMS matrix identified four OA factors，
588 including two primary OA (POA) factors, named as nitrogen-enriched hydrocarbon-like
589 OA (NHOA), and local primary OA (LOA), and two secondary OA factors which are a
590 less oxidized oxygenated OA (LO-OOA) and a more oxidized oxygenated OA
591 (MO-OOA), as shown in Fig. 10.
592 The NHOA factor had a low O/C ratio (0.19), and was abundant in $C_xH_y^+$ ions
593 (33.8%) and the NHOA time series also varied closely with those ions, representing its
594 features as traffic-related OA. In particular, the factor was rich in $C_xH_yN_p^+$ ions (43.1%),
595 as a result, it shows a much higher N/C ratio (0.26, Fig. 10a) than other factors, and
596 correlated well with CHN^+ (r = 0.91), CH_4N^+ (r = 0.95), CH_2N^+ (r = 0.85), and $C_2H_4N^+$
597 (r = 0.87) (Fig. 10b). The N-containing ions in the NHOA MS were dominated by the
598 reduced ions ($C_xH_yN^+$) rather than oxidized ones ($C_xH_yO_zN^+$), suggesting that amino
599 compounds were likely the major ON species, and was in consistent with our hypothesis
600 aforementioned in Section 3.6.1 that they were mainly from fossil fuel combustion
601 emissions. Nevertheless, future studies should be conducted to investigate in details the
602 contribution of fossil fuel combustion to the atmospheric ON species.
603 Another primary OA factor was defined as a local primary OA (LOA) contains
604 contributions from mixed anthropogenic emissions, such as cooking, coal combustion,
605 etc. LOA had a low O/C ratio of 0.19 and also contained mainly reduced $C_xH_y^+$ ions
606 (60.8%) as well, verifying its primary origin. Note its mass profile is characterized by
607 peaks at *m/z* 55 (significant $C_3H_3O^+$) and *m/z* 57 (significant $C_3H_5O^+$). The abundance of
608 $C_3H_3O^+$ at *m/z* 55 and $C_3H_5O^+$ at *m/z* 57 is a spectral feature of cooking OA, and the
609 overall COA MS and O/C ratios are also similar to the COA factors reported in other
610 studies, such as in Beijing. The LOA time series also correlated well with other
611 cooking-related marker ions, such as $C_5H_8O^+$ (r = 0.76), $C_6H_{10}O^+$ (r = 0.74), $C_7H_{12}O^+$ (r

= 0.67), consistent with the cooking OA from many previous studies (e.g., Sun et al., 2011b;Ge et al., 2012a). All these results indicate the LOA may have significant contributions from cooking activities. However, the ratio of LOA/$C_6H_{10}O^+$ (622.0) in this study was much higher than that obtained in winter in Fresno and New York City (~180), and also its mass fraction to the total OA was a few times higher than previous results, suggesting that it contains species from other primary sources rather than only cooking emissions.

The LO-OOA MS profile exhibited characteristics of oxidized OA with enhanced signals at *m/z* 29 (CHO^+), *m/z* 43 (mainly $C_2H_3O^+$) and other oxygenated ions. Tight correlations between time series of LO-OOA and CHO^+ (r = 0.92), and $C_2H_3O^+$ (r = 0.73) were also observed. Moreover, we also noticed relatively high signals of the BBOA tracer ions $C_2H_4O_2^+$ and $C_3H_5O_2^+$ in the LO-OOA MS, and found good correlations between LO-OOA and BBOA tracers (r = 0.87 with $C_2H_4O_2^+$, and r = 0.93 with $C_3H_5O_2^+$), indicating possible influence from biomass burning. Thus, we compared mass fraction of LO-OOA to total OA in different seasons assuming that LO-OOA contributions would increase in straw-burning seasons given that it could be influenced by BBOA. Figure S6 showed the mass fraction of four factors during straw-burning seasons (spring, summer) and non-straw burning seasons (fall, winter). No obvious difference for LO-OOA fraction was found. Furthermore, the O/C and OM/OC ratios were 0.53 and 1.95, corresponding to 0.34 and 1.62 if calculated by using method of Aiken et al. (2008), well within the O/C range of less-oxidized OA factors identified in other studies (Jimenez et al., 2009), but beyond the O/C range of typical BBOA (0.18 - 0.26) (He et al., 2010).

The MO-OOA factor had prominent peaks at *m/z* 28 (mainly CO^+) and *m/z* 44 (mainly CO_2^+), and was dominated by $C_xH_yO_1^+$ (36.6%) and $C_xH_yO_2^+$ ions (29.0%) (Fig. 10a). As a result, MO-OOA had a very high O/C ratio of 1.20, showing that it is heavily aged and processed OA component. Correspondingly, its time series correlated well with the secondary OA tracer ions, such as CO_2^+ (r = 0.93), $C_2H_4O^+$ (r = 0.67) and $C_2H_3O^+$ (r = 0.73) (Fig. 10b), etc.

The *f*44 (mass fraction of *m/z* 44 to the total OA) *vs.* *f*43 (mass fraction of *m/z* 43 to the total OA, defined by Ng et al. (2010)), can be used to investigate the degree of oxygenation of the identified factors. As presented in Fig. 11a, apart from NHOA, other three factors (LOA, LO-OOA and MO-OOA) all fall within the triangular region. MO-OOA located at the upper position with a higher *f*44 of 0.28, while LO-OOA located at the lower position of plot as it had a high fraction of *f*43 (0.09). This distribution of the four factors is also consistent with other studies.

The mass contributions of the four factors to total WSOA over the whole year are 23.9% for NHOA, 31.2% for LOA, 15.3% for LO-OOA and 29.7% for MO-OOA (Fig. 11b). POA (= NHOA + LOA) overweighed SOA (= LO-OOA + MO-OOA) mass, showing the dominant role of local anthropogenic emissions to the aerosol pollution in Changzhou, similar to that observed in Nanjing (Wang et al., 2016b). However, during spring and winter, SOA contributions dominate over POA, indicating significant SOA formation in particular the MO-OOA during cold seasons, which is in agreement with the OC/EC results.

3.7 Back trajectory clustering analysis

The Hybrid Single-particle Lagrangian Intergrated trajectory (HYSPLIT) model (Draxler et al., 2012) was used to investigate the origins of air masses based on the meteorological data available at the National Oceanic and Atmospheric Administration (NOAA) Global Data Assimilation System (GDAS). The 72h back trajectories of air parcels at 100 m above ground level in Changzhou were calculated at 8:00 local time (LT) throughout the campaign, and the results were presented in Fig. 12. The 4-, 5-, 4-, and 4-cluster solutions were adopted for spring, summer, fall and winter, respectively. During summer, air masses from southeast, east and west directions, passing over Shanghai and Anhui province, dominated the trajectories (75%) air masses. West and northwest air parcels dominated during winter, which may intercept air pollutants from Hebei and Anhui province. Considering the relatively short sampling days in each season, a more detailed discussion that is useful to distinguish contributions of local, regional and long-range transport to the air pollution, will be the subject of our future

671 work.

672

673 **4. Conclusions**

674 We presented here the comprehensive characterization results on the $PM_{2.5}$ samples
675 collected across one year in Changzhou City, located in the YRD region of China. The
676 species we quantified including WSIIs, trace metals, EC, WSOA, WIOA and also PAHs,
677 can reproduce on average ~80% mass of the $PM_{2.5}$ (108.3 μg m^{-3}). WSIIs were the major
678 component, accounting for 52.1% $PM_{2.5}$ mass, and NO_3^-, SO_4^{2-}, NH_4^+ were three most
679 abundant ions. The organic matter (the sum of WSOA and WIOA) occupied 21.5%
680 $PM_{2.5}$ mass, and EC accounted for ~5% $PM_{2.5}$ mass. Trace metal elements accounted for
681 ~5% and ~2.7% $PM_{2.5}$ mass during winter and spring. Total PAHs concentrations were
682 found to be at a relatively high concentration of 140.25 ng m^{-3} in winter, above three
683 times the average mass loading of 41.42 ng m^{-3} in spring, both with InP, BghiP and Chr
684 as the three most abundant PAHs. Average mass ratio of NO_3^-/SO_4^{2-} was 1.21,
685 suggesting a significant role of traffic emissions, which is in consistent with the source
686 analyses results based on the diagnostic ratios of the selected PAHs (BaP/BghiP,
687 Flua/(Flua+Pyr) and BaP/(BaP+Chr)). In addition, a high Cl^-/Na^+ ratio and the
688 diagnostic ratio of Phe/(Ant+Phe) indicated also the contribution from coal combustion,
689 in particular during winter.

690 In order to obtain further information regarding particle source, we analyzed the
691 WSOA using SP-AMS and conducted PMF analyses on the HRMS of WSOA. Four OA
692 factors including NHOA, LOA, LO-OOA and MO-OOA were identified. The mean
693 mass contribution of POA was larger than that of SOA, revealing that local
694 anthropogenic activities are the major drivers of PM pollution in Changzhou.
695 Nevertheless, during cold seasons, SOA mass contribution increased, indicating
696 significant role of secondarily formed species as well, thus reduction of air pollution in
697 Changzhou should be paid on the strict emission control of both primary particles and
698 the gaseous secondary aerosol precursors. One interesting finding in this work is the
699 enrichment of organic nitrogen species in WSOA, and source analysis indicates that

traffic emissions can be a significant contributor to these species, which warrants more detailed investigations in the future. Also, more offline samples should be collected to achieve a more robust PMF analyses. Simultaneous online AMS measurement on the fine particles and measurements of gaseous species (SO_2, NO_2, O_3, CO and some volatile organic compounds) are also essential to better understand the aerosol characteristics, and to implement proper measures to abate the air pollution in this region.

Acknowledgements

This work was supported the Natural Science Foundation of China (Grant Nos. (21407079 and 91544220), the Jiangsu National Science Foundation (BK20150042), the Specially-Appointed Professors Foundation and Jiangsu Innovation and Entrepreneurship Program (for X.G.), and the Major Research Development Program of Jiangsu Province (BE2016657 and BY2016030-15). We would also like to acknowledge Mr. Gang Li from Chinese academy of Science for providing us the OC/EC measurements.

References:

Aiken, A. C., Decarlo, P. F., Kroll, J. H., Worsnop, D. R., Huffman, J. A., Docherty, K. S., Ulbrich, I. M., Mohr, C., Kimmel, J. R., Sueper, D., Sun, Y., Zhang, Q., Trimborn, A., Northway, M., Ziemann, P. J., Canagaratna, M. R., Onasch, T. B., Alfarra, M. R., Prevot, A. S. H., Dommen, J., Duplissy, J., Metzger, A., Baltensperger, U., and Jimenez, J. L.: O/C and OM/OC ratios of primary, secondary, and ambient organic aerosols with high-resolution time-of-flight aerosol mass spectrometry, Environ. Sci. Technol., 42, 4478-4485, doi: 10.1021/Es703009q, 2008.

Anderson, J. O., Thundiyil, J. G., and Stolbach, A.: Clearing the air: A review of the effects of particulate matter air pollution on human health, J. Med. Toxicol., 8, 166-175, doi: 10.1007/s13181-011-0203-1, 2012.

Arimoto, R., Duce, R. A., Savoie, D. L., Prospero, J. M., Talbot, R., Cullen, J. D., Tomza, U., Lewis, N. F., and Ray, B. J.: Relationships among aerosol constituents from Asia and the North Pacific during PEM-West A, J. Geophys. Res. -Atmos., 101, 2011-2023, doi: 10.1029/95JD01071, 1996.

Bozzetti, C., Sosedova, Y., Xiao, M., Daellenbach, K. R., Ulevicius, V., Dudoitis, V., Mordas,

733 G., Byčenkienė, S., Plauškaitė, K., Vlachou, A., Golly, B., Chazeau, B., Besombes, J. L.,
734 Baltensperger, U., Jaffrezo, J. L., Slowik, J. G., El Haddad, I., and Prévôt, A. S. H.: Argon
735 offline-AMS source apportionment of organic aerosol over yearly cycles for an urban, rural, and
736 marine site in northern Europe, Atmos. Chem. Phys., 17, 117-141, doi:
737 10.5194/acp-17-117-2017, 2017.

738 Canagaratna, M. R., Jayne, J. T., Jimenez, J. L., Allan, J. D., Alfarra, M. R., Zhang, Q., Onasch,
739 T. B., Drewnick, F., Coe, H., Middlebrook, A., Delia, A., Williams, L. R., Trimborn, A. M.,
740 Northway, M. J., DeCarlo, P. F., Kolb, C. E., Davidovits, P., and Worsnop, D. R.: Chemical and
741 microphysical characterization of ambient aerosols with the aerodyne aerosol mass spectrometer,
742 Mass Spectrom Rev, 26, 185-222, doi: 10.1002/Mas.20115, 2007.

743 Canagaratna, M. R., Jimenez, J. L., Kroll, J. H., Chen, Q., Kessler, S. H., Massoli, P.,
744 Hildebrandt Ruiz, L., Fortner, E., Williams, L. R., Wilson, K. R., Surratt, J. D., Donahue, N. M.,
745 Jayne, J. T., and Worsnop, D. R.: Elemental ratio measurements of organic compounds using
746 aerosol mass spectrometry: characterization, improved calibration, and implications, Atmos.
747 Chem. Phys., 15, 253-272, doi: 10.5194/acp-15-253-2015, 2015.

748 Cao, J. J., Xu, H. M., Xu, Q., Chen, B. H., and Kan, H. D.: Fine particulate matter constituents
749 and cardiopulmonary mortality in a heavily polluted Chinese city, Environ. Health Persp., 120,
750 373-378, doi: 10.1289/ehp.1103671, 2012.

751 Cheng, Y., He, K. B., Du, Z. Y., Zheng, M., Duan, F. K., and Ma, Y. L.: Humidity plays an
752 important role in the PM(2).(5) pollution in Beijing, Environ. Pollut., 197, 68-75, doi:
753 10.1016/j.envpol.2014.11.028, 2015.

754 Chow, J. C., Watson, J. G., Chen, L. W. A., Arnott, W. P., Moosmüller, H., and Fung, K.:
755 Equivalence of elemental carbon by thermal/optical reflectance and transmittance with different
756 temperature protocols, Environ. Sci. Technol. , 38, 4414-4422, doi: 10.1021/es034936u, 2004.

757 Chow, J. C., Watson, J. G., Louie, P. K., Chen, L. W., and Sin, D.: Comparison of PM2.5 carbon
758 measurement methods in Hong Kong, China, Environ. Pollut., 137, 334-344, doi:
759 10.1016/j.envpol.2005.01.006, 2005.

760 Daellenbach, K. R., Bozzetti, C., Křepelová, A., Canonaco, F., Wolf, R., Zotter, P., Fermo, P.,
761 Crippa, M., Slowik, J. G., Sosedova, Y., Zhang, Y., Huang, R. J., Poulain, L., Szidat, S.,
762 Baltensperger, U., El Haddad, I., and Prévôt, A. S. H.: Characterization and source
763 apportionment of organic aerosol using offline aerosol mass spectrometry, Atmos. Meas. Tech.,
764 9, 23-39, doi: 10.5194/amt-9-23-2016, 2016.

765 Ding, A. J., Fu, C. B., Yang, X. Q., Sun, J. N., Zheng, L. F., Xie, Y. N., Herrmann, E., Nie, W.,
766 Petaja, T., Kerminen, V. M., and Kulmala, M.: Ozone and fine particle in the western Yangtze
767 River Delta: an overview of 1 yr data at the SORPES station, Atmos. Chem. Phys., 13,
768 5813-5830, doi: 10.5194/acp-13-5813-2013, 2013.

769 Draxler, R., Stunder, B., Rolph, G., Stein, A., and Taylor, A.: HYSPLIT4 user's guide, version 4,

770 report, NOAA, Silver Spring, MD, doi, 2012.

771 Drewnick, F.: Speciation analysis in on-line aerosol mass spectrometry, Anal. Bioanal. Chem.,
772 404, 2127-2131, doi: 10.1007/s00216-012-6295-x, 2012.

773 Duan, F., Liu, X., He, K., and Dong, S.: Measurements and characteristics of
774 nitrogen-containing compounds in atmospheric particulate matter in Beijing, China, Bull.
775 Environ. Contam. Toxicol., 82, 332-337, doi: 10.1007/s00128-008-9560-0, 2009.

776 Duan, J., Tan, J., Wang, S., Chai, F., He, K., and Hao, J.: Roadside, urban, and rural comparison
777 of size distribution characteristics of PAHs and carbonaceous components of Beijing, China, J.
778 Atmos. Chem., 69, 337-349, doi: 10.1007/s10874-012-9242-5, 2012.

779 Dzepina, K., Arey, J., Marr, L. C., Worsnop, D. R., Salcedo, D., Zhang, Q., Onasch, T. B.,
780 Molina, L. T., Molina, M. J., and Jimenez, J. L.: Detection of particle-phase polycyclic aromatic
781 hydrocarbons in Mexico City using an aerosol mass spectrometer, Int. J. Mass Spectrom., 263,
782 152-170, doi: 10.1016/j.ijms.2007.01.010, 2007.

783 Fan, J., Yue, X., Jing, Y., Chen, Q., and Wang, S.: Online monitoring of water-soluble ionic
784 composition of PM10 during early summer over Lanzhou City, J. Environ. Sci., 26, 353-361, doi:
785 10.1016/s1001-0742(13)60431-3, 2014.

786 Feng, J., Hu, J., Xu, B., Hu, X., Sun, P., Han, W., Gu, Z., Yu, X., and Wu, M.: Characteristics
787 and seasonal variation of organic matter in PM2.5 at a regional background site of the Yangtze
788 River Delta region, China, Atmos. Environ., 123, 288-297, doi: 10.1016/j.atmosenv.2015.08.019,
789 2015.

790 Feng, Y., Chen, Y., Guo, H., Zhi, G., Xiong, S., Li, J., Sheng, G., and Fu, J.: Characteristics of
791 organic and elemental carbon in PM2.5 samples in Shanghai, China, Atmos. Res., 92, 434-442,
792 doi: 10.1016/j.atmosres.2009.01.003, 2009.

793 Fu, H., Zhang, M., Li, W., Chen, J., Wang, L., Quan, X., and Wang, W.: Morphology,
794 composition and mixing state of individual carbonaceous aerosol in urban Shanghai, Atmos.
795 Chem. Phys., 12, 693-707, doi: 10.5194/acp-12-693-2012, 2012.

796 Ge, X., Wexler, A. S., and Clegg, S. L.: Atmospheric amines - Part II. Thermodynamic
797 properties and gas/particle partitioning, Atmos. Environ., 45, 561-577, doi: DOI
798 10.1016/j.atmosenv.2010.10.013, 2011a.

799 Ge, X., Wexler, A. S., and Clegg, S. L.: Atmospheric amines - Part I. A review, Atmos. Environ.,
800 45, 524-546, doi: DOI 10.1016/j.atmosenv.2010.10.012, 2011b.

801 Ge, X., Setyan, A., Sun, Y., and Zhang, Q.: Primary and secondary organic aerosols in Fresno,
802 California during wintertime: Results from high resolution aerosol mass spectrometry, J.
803 Geophys. Res. -Atmos., 117, D19301, doi: 10.1029/2012jd018026, 2012a.

804 Ge, X., Zhang, Q., Sun, Y., Ruehl, C. R., and Setyan, A.: Effect of aqueous-phase processing on

aerosol chemistry and size distributions in Fresno, California, during wintertime, Environ. Chem., 9, 221-235, doi: 10.1071/EN11168, 2012b.

Ge, X., Shaw, S. L., and Zhang, Q.: Toward understanding amines and their degradation products from postcombustion CO2 capture processes with aerosol mass spectrometry, Environ. Sci. Technol., 48, 5066-5075, doi: 10.1021/es4056966, 2014.

Ge, X., Wang, J., Zhang, Z., Wang, X., and Chen, M.: Thermodynamic modeling of electrolyte solutions by a hybrid ion-interaction and solvation (HIS) model, Calphad, 48, 79-88, doi: 10.1016/j.calphad.2014.11.001, 2015.

Gu, J., Bai, Z., Liu, A., Wu, L., Xie, Y., Li, W., Dong, H., and Zhang, X.: Characterization of atmospheric organic carbon and element carbon of PM2.5 and PM10 at Tianjin, China, Aerosol Air Qual. Res., 10, 167-176, doi: 10.4209/aaqr.2009.12.0080, 2010.

Gu, J., Du, S., Han, D., Hou, L., Yi, J., Xu, J., Liu, G., Han, B., Yang, G., and Bai, Z.-P.: Major chemical compositions, possible sources, and mass closure analysis of PM2.5 in Jinan, China, Air Qual. Atmos. Health, 7, 251-262, doi: 10.1007/s11869-013-0232-9, 2014.

He, J., Fan, S., Meng, Q., Sun, Y., Zhang, J., and Zu, F.: Polycyclic aromatic hydrocarbons (PAHs) associated with fine particulate matters in Nanjing, China: Distributions, sources and meteorological influences, Atmos. Environ., 89, 207-215, doi: 10.1016/j.atmosenv.2014.02.042, 2014.

He, L. Y., Lin, Y., Huang, X. F., Guo, S., Xue, L., Su, Q., Hu, M., Luan, S. J., and Zhang, Y. H.: Characterization of high-resolution aerosol mass spectra of primary organic aerosol emissions from Chinese cooking and biomass burning, Atmos. Chem. Phys., 10, 11535-11543, doi: 10.5194/acp-10-11535-2010, 2010.

Heal, M. R., Kumar, P., and Harrison, R. M.: Particles, air quality, policy and health, Chem. Soc. Rev., doi, 2012.

Ho, K. F., Ho, S. S. H., Huang, R.-J., Liu, S. X., Cao, J.-J., Zhang, T., Chuang, H.-C., Chan, C. S., Hu, D., and Tian, L.: Characteristics of water-soluble organic nitrogen in fine particulate matter in the continental area of China, Atmos. Environ., 106, 252-261, doi: 10.1016/j.atmosenv.2015.02.010, 2015.

Hu, J., Ying, Q., Wang, Y., and Zhang, H.: Characterizing multi-pollutant air pollution in China: Comparison of three air quality indices, Environ. Int., 84, 17-25, doi: 10.1016/j.envint.2015.06.014, 2015.

Hu, W., Hu, M., Hu, W., Jimenez, J. L., Yuan, B., Chen, W., Wang, M., Wu, Y., Chen, C., Wang, Z., Peng, J., Zeng, L., and Shao, M.: Chemical composition, sources, and aging process of submicron aerosols in Beijing: Contrast between summer and winter, J. Geophys. Res. -Atmos., 121, 2015JD024020, doi: 10.1002/2015JD024020, 2016.

Hu, X., Zhang, Y., Ding, Z., Wang, T., Lian, H., Sun, Y., and Wu, J.: Bioaccessibility and health

841 risk of arsenic and heavy metals (Cd, Co, Cr, Cu, Ni, Pb, Zn and Mn) in TSP and PM2.5 in
842 Nanjing, China, Atmos. Environ., 57, 146-152, doi: 10.1016/j.atmosenv.2012.04.056, 2012.

843 Huang, R., Zhang, Y., Bozzetti, C., Ho, K., Cao, J., Han, Y., Daellenbach, K. R., Slowik, J. G.,
844 Platt, S. M., Canonaco, F., Zotter, P., Wolf, R., Pieber, S. M., Bruns, E. A., Crippa, M., Ciarelli,
845 G., Piazzalunga, A., Schwikowski, M., Abbaszade, G., Schnelle-Kreis, J., Zimmermann, R., An,
846 Z., Szidat, S., Baltensperger, U., Haddad, I. E., and Prevot, A. S. H.: High secondary aerosol
847 contribution to particulate pollution during haze events in China, Nature, 514, 218-222, doi:
848 10.1038/nature13774, 2014.

849 Huang, T., Chen, J., Zhao, W., Cheng, J., and Cheng, S.: Seasonal variations and correlation
850 analysis of water-soluble inorganic ions in PM2.5 in Wuhan, 2013, Atmosphere, 7, 49, doi:
851 10.3390/atmos7040049, 2016.

852 Huang, X. F., He, L. Y., Hu, M., Canagaratna, M. R., Sun, Y., Zhang, Q., Zhu, T., Xue, L., Zeng,
853 L. W., Liu, X. G., Zhang, Y. H., Jayne, J. T., Ng, N. L., and Worsnop, D. R.: Highly
854 time-resolved chemical characterization of atmospheric submicron particles during 2008 Beijing
855 Olympic Games using an Aerodyne High-Resolution Aerosol Mass Spectrometer, Atmos. Chem.
856 Phys., 10, 8933-8945, doi: 10.5194/acp-10-8933-2010, 2010.

857 Jimenez, J. L., Canagaratna, M. R., Donahue, N. M., Prevot, A. S. H., Zhang, Q., Kroll, J. H.,
858 DeCarlo, P. F., Allan, J. D., Coe, H., Ng, N. L., Aiken, A. C., Docherty, K. S., Ulbrich, I. M.,
859 Grieshop, A. P., Robinson, A. L., Duplissy, J., Smith, J. D., Wilson, K. R., Lanz, V. A., Hueglin,
860 C., Sun, Y. L., Tian, J., Laaksonen, A., Raatikainen, T., Rautiainen, J., Vaattovaara, P., Ehn, M.,
861 Kulmala, M., Tomlinson, J. M., Collins, D. R., Cubison, M. J., Dunlea, E. J., Huffman, J. A.,
862 Onasch, T. B., Alfarra, M. R., Williams, P. I., Bower, K., Kondo, Y., Schneider, J., Drewnick, F.,
863 Borrmann, S., Weimer, S., Demerjian, K., Salcedo, D., Cottrell, L., Griffin, R., Takami, A.,
864 Miyoshi, T., Hatakeyama, S., Shimono, A., Sun, J. Y., Zhang, Y. M., Dzepina, K., Kimmel, J. R.,
865 Sueper, D., Jayne, J. T., Herndon, S. C., Trimborn, A. M., Williams, L. R., Wood, E. C.,
866 Middlebrook, A. M., Kolb, C. E., Baltensperger, U., and Worsnop, D. R.: Evolution of organic
867 aerosols in the atmosphere, Science, 326, 1525-1529, doi: 10.1126/science.1180353, 2009.

868 Khalili, N. R., Scheff, P. A., and Holsen, T. M.: PAH source fingerprints for coke ovens, diesel
869 and, gasoline engines, highway tunnels, and wood combustion emissions, Atmos. Environ., 29,
870 533-542, doi: 10.1016/1352-2310(94)00275-P, 1995.

871 Kong, S., Ding, X., Bai, Z., Han, B., Chen, L., Shi, J., and Li, Z.: A seasonal study of polycyclic
872 aromatic hydrocarbons in PM(2.5) and PM(2.5-10) in five typical cities of Liaoning Province,
873 China, J. Hazard. Mater., 183, 70-80, doi: 10.1016/j.jhazmat.2010.06.107, 2010.

874 Kong, S., Li, X., Li, L., Yin, Y., Chen, K., Yuan, L., Zhang, Y., Shan, Y., and Ji, Y.: Variation
875 of polycyclic aromatic hydrocarbons in atmospheric PM2.5 during winter haze period around
876 2014 Chinese Spring Festival at Nanjing: Insights of source changes, air mass direction and
877 firework particle injection, Sci. Total Environ., 520, 59-72, doi: 10.1016/j.scitotenv.2015.03.001,
878 2015.

879 Kulmala, M., Lappalainen, H. K., Petäjä, T., Kurten, T., Kerminen, V. M., Viisanen, Y., Hari, P.,
880 Sorvari, S., Bäck, J., Bondur, V., Kasimov, N., Kotlyakov, V., Matvienko, G., Baklanov, A.,
881 Guo, H. D., Ding, A., Hansson, H. C., and Zilitinkevich, S.: Introduction: The Pan-Eurasian
882 Experiment (PEEX) – multidisciplinary, multiscale and multicomponent research and
883 capacity-building initiative, Atmos. Chem. Phys., 15, 13085-13096, doi:
884 10.5194/acp-15-13085-2015, 2015.

885 Lee, A. K. Y., Willis, M. D., Healy, R. M., Onasch, T. B., and Abbatt, J. P. D.: Mixing state of
886 carbonaceous aerosol in an urban environment: single particle characterization using the soot
887 particle aerosol mass spectrometer (SP-AMS), Atmos. Chem. Phys., 15, 1823-1841, doi:
888 10.5194/acp-15-1823-2015, 2015.

889 Li, B., Zhang, J., Zhao, Y., Yuan, S., Zhao, Q., Shen, G., and Wu, H.: Seasonal variation of
890 urban carbonaceous aerosols in a typical city Nanjing in Yangtze River Delta, China, Atmos.
891 Environ., 106, 223-231, doi: 10.1016/j.atmosenv.2015.01.064, 2015.

892 Liu, G., Li, J., Wu, D., and Xu, H.: Chemical composition and source apportionment of the
893 ambient PM2.5 in Hangzhou, China, Particuology, 18, 135-143, doi:
894 10.1016/j.partic.2014.03.011, 2015.

895 Meng, C. C., Wang, L. T., Zhang, F. F., Wei, Z., Ma, S. M., Ma, X., and Yang, J.:
896 Characteristics of concentrations and water-soluble inorganic ions in PM2.5 in Handan City,
897 Hebei province, China, Atmos. Res., 171, 133-146, doi: 10.1016/j.atmosres.2015.12.013, 2016.

898 Mihara, T., and Mochida, M.: Characterization of Solvent-Extractable Organics in Urban
899 Aerosols Based on Mass Spectrum Analysis and Hygroscopic Growth Measurement, Environ.
900 Sci. Technol., 45, 9168-9174, doi: 10.1021/es201271w, 2011.

901 Mirante, F., Salvador, P., Pio, C., Alves, C., Artiñano, B., Caseiro, A., and Revuelta, M. A.: Size
902 fractionated aerosol composition at roadside and background environments in the Madrid urban
903 atmosphere, Atmos. Res., 138, 278-292, doi: 10.1016/j.atmosres.2013.11.024, 2014.

904 Ng, N. L., Canagaratna, M. R., Zhang, Q., Jimenez, J. L., Tian, J., Ulbrich, I. M., Kroll, J. H.,
905 Docherty, K. S., Chhabra, P. S., Bahreini, R., Murphy, S. M., Seinfeld, J. H., Hildebrandt, L.,
906 Donahue, N. M., DeCarlo, P. F., Lanz, V. A., Prévôt, A. S. H., Dinar, E., Rudich, Y., and
907 Worsnop, D. R.: Organic aerosol components observed in Northern Hemispheric datasets from
908 Aerosol Mass Spectrometry, Atmos. Chem. Phys., 10, 4625-4641, doi:
909 10.5194/acp-10-4625-2010, 2010.

910 Ng, N. L., Canagaratna, M. R., Jimenez, J. L., Zhang, Q., Ulbrich, I. M., and Worsnop, D. R.:
911 Real-time methods for estimating organic component mass concentrations from aerosol mass
912 spectrometer data, Environ. Sci. Technol., 45, 910-916, doi: Doi 10.1021/Es102951k, 2011.

913 Onasch, T. B., Trimborn, A., Fortner, E. C., Jayne, J. T., Kok, G. L., Williams, L. R., Davidovits,
914 P., and Worsnop, D. R.: Soot particle aerosol mass spectrometer: Development, validation, and
915 initial application, Aerosol Sci. Tech., 46, 804-817, doi: 10.1080/02786826.2012.663948, 2012.

916 Pan, Y., Tian, S., Liu, D., Fang, Y., Zhu, X., Zhang, Q., Zheng, B., Michalski, G., and Wang, Y.:
917 Fossil Fuel Combustion-Related Emissions Dominate Atmospheric Ammonia Sources during
918 Severe Haze Episodes: Evidence from 15N-Stable Isotope in Size-Resolved Aerosol
919 Ammonium, Environ. Sci. Technol., 50, 8049-8056, doi: 10.1021/acs.est.6b00634, 2016.

920 Qi, L., Chen, M., Ge, X., Zhang, Y., and Guo, B.: Seasonal variations and sources of 17 aerosol
921 metal elements in suburban Nanjing, China, Atmosphere, 7, 153, doi, 2016a.

922 Qi, L., Zhang, Y., Ma, Y., Chen, M., Ge, X., Ma, Y., Zheng, J., Wang, Z., and Li, S.: Source
923 identification of trace elements in the atmosphere during the second Asian Youth Games in
924 Nanjing, China: Influence of control measures on air quality, Atmos. Pollut. Res., 7, 547-556,
925 doi: 10.1016/j.apr.2016.01.003, 2016b.

926 Qiao, T., Zhao, M., Xiu, G., and Yu, J.: Seasonal variations of water soluble composition
927 (WSOC, Hulis and WSIIs) in PM1 and its implications on haze pollution in urban Shanghai,
928 China, Atmos. Environ., 123, 306-314, doi: 10.1016/j.atmosenv.2015.03.010, 2015.

929 Saldarriaga-Noreña, H., López-Márquez, R., Murillo-Tovar, M., Hernández-Mena, L.,
930 Ospina-Noreña, E., Sánchez-Salinas, E., Waliszewski, S., and Montiel-Palma, S.: Analysis of
931 PAHs associated with particulate matter PM2.5 in two places at the city of Cuernavaca, Morelos,
932 México, Atmosphere, 6, 1259-1270, doi: 10.3390/atmos6091259, 2015.

933 Shen, G. F., Yuan, S. Y., Xie, Y. N., Xia, S. J., Li, L., Yao, Y. K., Qiao, Y. Z., Zhang, J., Zhao,
934 Q. Y., Ding, A. J., Li, B., and Wu, H. S.: Ambient levels and temporal variations of PM2.5 and
935 PM10 at a residential site in the mega-city, Nanjing, in the western Yangtze River Delta, China,
936 J. Environ. Sci. Health A: Tox. Hazard. Subst. Environ..Eng., 49, 171-178, doi:
937 10.1080/10934529.2013.838851, 2014.

938 Shi, J., Gao, H., Qi, J., Zhang, J., and Yao, X.: Sources, compositions, and distributions of
939 water-soluble organic nitrogen in aerosols over the China Sea, J. Geophys. Res. -Atmos., 115,
940 doi: 10.1029/2009jd013238, 2010.

941 Sun, Y., Zhang, Q., Zheng, M., Ding, X., Edgerton, E. S., and Wang, X.: Characterization and
942 source apportionment of water-soluble organic matter in atmospheric fine particles (PM2.5) with
943 high-resolution aerosol mass spectrometry and GC-MS, Environ. Sci. Technol., 45, 4854-4861,
944 doi: 10.1021/es200162h, 2011a.

945 Sun, Y., Jiang, Q., Wang, Z., Fu, P., Li, J., Yang, T., and Yin, Y.: Investigation of the sources
946 and evolution processes of severe haze pollution in Beijing in January 2013, J. Geophys. Res.
947 -Atmos., 119, 4380-4398, doi: 10.1002/2014jd021641, 2014.

948 Sun, Y., Du, W., Fu, P., Wang, Q., Li, J., Ge, X., Zhang, Q., Zhu, C., Ren, L., Xu, W., Zhao, J.,
949 Han, T., Worsnop, D. R., and Wang, Z.: Primary and secondary aerosols in Beijing in winter:
950 sources, variations and processes, Atmos. Chem. Phys., 16, 8309-8329, doi:
951 10.5194/acp-16-8309-2016, 2016.

952 Sun, Y. L., Zhang, Q., Schwab, J. J., Demerjian, K. L., Chen, W. N., Bae, M. S., Hung, H. M.,
953 Hogrefe, O., Frank, B., Rattigan, O. V., and Lin, Y. C.: Characterization of the sources and
954 processes of organic and inorganic aerosols in New York city with a high-resolution
955 time-of-flight aerosol mass apectrometer, Atmos. Chem. Phys., 11, 1581-1602, doi:
956 10.5194/acp-11-1581-2011, 2011b.

957 Szabó, J., Nagy, A. S., and Erdős, J.: Ambient concentrations of PM10, PM10-bound polycyclic
958 aromatic hydrocarbons and heavy metals in an urban site of Győr, Hungary, Air Qual. Atmos.
959 Health, 8, 229-241, doi: 10.1007/s11869-015-0318-7, 2015.

960 Ulbrich, I. M., Canagaratna, M. R., Zhang, Q., Worsnop, D. R., and Jimenez, J. L.:
961 Interpretation of organic components from Positive Matrix Factorization of aerosol mass
962 spectrometric data, Atmos. Chem. Phys., 9, 2891-2918, doi: 10.5194/acp-9-2891-2009, 2009.

963 Violaki, K., and Mihalopoulos, N.: Water-soluble organic nitrogen (WSON) in size-segregated
964 atmospheric particles over the Eastern Mediterranean, Atmos. Environ., 44, 4339-4345 doi,
965 2010.

966 Wang, F., Lin, T., Feng, J., Fu, H., and Guo, Z.: Source apportionment of polycyclic aromatic
967 hydrocarbons in PM2.5 using positive matrix factorization modeling in Shanghai, China,
968 Environ. Sci. Process Impacts, 17, 197-205, doi: 10.1039/c4em00570h, 2015.

969 Wang, F., Guo, Z., Lin, T., and Rose, N. L.: Seasonal variation of carbonaceous pollutants in
970 PM2.5 at an urban 'supersite' in Shanghai, China, Chemosphere, 146, 238-244, doi:
971 10.1016/j.chemosphere.2015.12.036, 2016a.

972 Wang, G., Kawamura, K., Lee, S., Ho, K., and Cao, J.: Molecular, seasonal, and spatial
973 distributions of organic aerosols from fourteen Chinese cities, Environ. Sci. Technol., 40,
974 4619-4625, doi: 10.1021/es060291x, 2006a.

975 Wang, J., Geng, N. B., Xu, Y. F., Zhang, W. D., Tang, X. Y., and Zhang, R. Q.: PAHs in PM2.5
976 in Zhengzhou: concentration, carcinogenic risk analysis, and source apportionment, Environ.
977 Monit. Assess., 186, 7461-7473, doi: 10.1007/s10661-014-3940-1, 2014.

978 Wang, J., Ge, X., Chen, Y., Shen, Y., Zhang, Q., Sun, Y., Xu, J., Ge, S., Yu, H., and Chen, M.:
979 Highly time-resolved urban aerosol characteristics during springtime in Yangtze River Delta,
980 China: insights from soot particle aerosol mass spectrometry, Atmos. Chem. Phys., 16,
981 9109-9127, doi: 10.5194/acp-16-9109-2016, 2016b.

982 Wang, J., Onasch, T. B., Ge, X., Collier, S., Zhang, Q., Sun, Y., Yu, H., Chen, M., Prévôt, A. S.
983 H., and Worsnop, D. R.: Observation of fullerene foot in eastern China, Environ. Sci. Technol.
984 Lett., 3, 121-126, doi: 10.1021/acs.estlett.6b00044, 2016c.

985 Wang, T., Jiang, F., Deng, J., Shen, Y., Fu, Q., Wang, Q., Fu, Y., Xu, J., and Zhang, D.: Urban
986 air quality and regional haze weather forecast for Yangtze River Delta region, Atmos. Environ.,
987 58, 70-83, doi: 10.1016/j.atmosenv.2012.01.014, 2012.

Wang, Y., Zhuang, G., Zhang, X., Huang, K., Xu, C., Tang, A., Chen, J., and An, Z.: The ion chemistry, seasonal cycle, and sources of PM2.5 and TSP aerosol in Shanghai, Atmos. Environ., 40, 2935-2952, doi: 10.1016/j.atmosenv.2005.12.051, 2006b.

Xu, J., Zhang, Q., Li, X., Ge, X., Xiao, C., Ren, J., and Qin, D.: Dissolved organic matter and inorganic Ions in a central Himalayan glacier—Insights into chemical composition and atmospheric sources, Environ. Sci. Technol., 47, 6181-6188, doi: 10.1021/es4009882, 2013.

Xu, J., Zhang, Q., Chen, M., Ge, X., Ren, J., and Qin, D.: Chemical composition, sources, and processes of urban aerosols during summertime in northwest China: insights from high-resolution aerosol mass spectrometry, Atmos. Chem. Phys., 14, 12593-12611, doi: 10.5194/acp-14-12593-2014, 2014.

Xu, J., Zhang, Q., Wang, Z., Yu, G., Ge, X., and Qin, X.: Chemical composition and size distribution of summertime PM2.5 at a high altitude remote location in the northeast of the Qinghai–Xizang (Tibet) Plateau: insights into aerosol sources and processing in free troposphere, Atmos. Chem. Phys., 15, 5069-5081, doi: 10.5194/acp-15-5069-2015, 2015.

Xu, L., Guo, H., Weber, R. J., and Ng, N. L.: Chemical Characterization of Water-Soluble Organic Aerosol in Contrasting Rural and Urban Environments in the Southeastern United States, Environ. Sci. Technol., 51, 78-88, doi: 10.1021/acs.est.6b05002, 2017.

Ye, X. N., Ma, Z., Hu, D. W., Yang, X., and Chen, J. M.: Size-resolved hygroscopicity of submicrometer urban aerosols in Shanghai during wintertime, Atmos. Res., 99, 353-364, doi: 10.1016/j.atmosres.2010.11.008, 2011.

Zhang, Q., Jimenez, J. L., Canagaratna, M. R., Allan, J. D., Coe, H., Ulbrich, I., Alfarra, M. R., Takami, A., Middlebrook, A. M., Sun, Y. L., Dzepina, K., Dunlea, E., Docherty, K., DeCarlo, P. F., Salcedo, D., Onasch, T., Jayne, J. T., Miyoshi, T., Shimono, A., Hatakeyama, S., Takegawa, N., Kondo, Y., Schneider, J., Drewnick, F., Borrmann, S., Weimer, S., Demerjian, K., Williams, P., Bower, K., Bahreini, R., Cottrell, L., Griffin, R. J., Rautiainen, J., Sun, J. Y., Zhang, Y. M., and Worsnop, D. R.: Ubiquity and dominance of oxygenated species in organic aerosols in anthropogenically-influenced Northern Hemisphere midlatitudes, Geophys. Res. Lett., 34, n/a-n/a, doi: 10.1029/2007gl029979, 2007a.

Zhang, Q., Jimenez, J. L., Worsnop, D. R., and Canagaratna, M.: A case study of urban particle acidity and its influence on secondary organic aerosol, Environ. Sci. Technol., 41, 3213-3219, doi: 10.1021/Es061812j, 2007b.

Zhang, Q., Jimenez, J. L., Canagaratna, M. R., Ulbrich, I. M., Ng, N. L., Worsnop, D. R., and Sun, Y.: Understanding atmospheric organic aerosols via factor analysis of aerosol mass spectrometry: a review, Anal. Bioanal. Chem., 401, 3045-3067, doi: 10.1007/s00216-011-5355-y, 2011.

Zhang, R., Jing, J., Tao, J., Hsu, S. C., Wang, G., Cao, J., Lee, C. S. L., Zhu, L., Chen, Z., Zhao, Y., and Shen, Z.: Chemical characterization and source apportionment of PM2.5 in Beijing:

seasonal perspective, Atmos. Chem. Phys., 13, 7053-7074, doi: 10.5194/acp-13-7053-2013, 2013.

Zhang, Y. J., Tang, L., Yu, H., Wang, Z., Sun, Y., Qin, W., Chen, W., Chen, C., Ding, A., Wu, J., Ge, S., Chen, C., and Zhou, H.-c.: Chemical composition, sources and evolution processes of aerosol at an urban site in Yangtze River Delta, China during wintertime, Atmos. Environ., 123, 339-349, doi: 10.1016/j.atmosenv.2015.08.017, 2016.

Zhao, M., Huang, Z., Qiao, T., Zhang, Y., Xiu, G., and Yu, J.: Chemical characterization, the transport pathways and potential sources of PM2.5 in Shanghai: Seasonal variations, Atmos. Res., 158-159, 66-78, doi: 10.1016/j.atmosres.2015.02.003, 2015.

Zhou, J., Xing, Z., Deng, J., and Du, K.: Characterizing and sourcing ambient PM2.5 over key emission regions in China I: Water-soluble ions and carbonaceous fractions, Atmos. Environ., 135, 20-30, doi: 10.1016/j.atmosenv.2016.03.054, 2016.

1039 Table 1. Average meteorological parameters during four seasons

Parameters	Spring	Summer	Fall	Winter
RH (%)	57.3±11.4	61.1±11.8	65.5±10.9	62.3±10.6
T(^{o}C)	13.1±4.0	32.1±4.3	21.6±2.3	5.6±1.8
WS(m s^{-1})	1.1±0.4	1.6±0.6	0.9±0.4	0.9±0.3
WD[a]	SE	E,W,SE	E	W,NW,SE

1040 [a] Refer to prevailing wind directions, E—East, SE—Southeast, W—West,
1041 NW-Northwest.
1042

1043 Table 2. Summary of aerosol species, analytical methods, measurement uncertainties
1044 and the method detection limits (MDLs).

Species	Analytical methods	Uncertainties	MDLs
Water soluble ions	Ion chromatography	3.5 - 7.0%	3 - 20 μg L^{-1}
Trace elements	ICP-OES	10.3 - 18.5%	-
OC, EC	Thermal-Optical Carbon Analyzer	<12%	30 - 80 ng m^{-3} for OC and 30 ng m^{-3} for EC (Mirante et al., 2014)
WSOC	TOC analyzer	3.4 - 6.0%	5.0 μg L^{-1}
PAH	GC-MS	20%	2 - 5μg L^{-1}
OM/OC ratio	SP-AMS	6% (Aiken et al., 2008)	-
WSOA	SP-AMS,TOC	6.9 - 8.5%	-

1045

Table 3. Summary of the mean concentrations (with one standard deviation) and mass fractions for $PM_{2.5}$ and all quantified components in four seasons and the whole sampling period, respectively.

Species ($\mu g\ m^{-3}$)	Spring	Summer	Fall	Winter	Annual
$PM_{2.5}$	**106.0±24.4**	**80.9±37.7**	**103.3±28.2**	**126.9±50.4**	**108.3±40.8**
WSIIs	**66.5±17.2**	**35.0±20.2**	**51.0±17.2**	**66.8±23.6**	**56.4**±22.9
Sulfate	17.3±4.8	15.8±9.8	17.2±6.2	18.7±7.6	17.5±7.1
Nitrate	26.4±8.7	6.8±6.2	17.0±9.0	24.1±11.8	19.3±11.6
Ammonium	14.8±4.2	8.2±4.3	11.2±3.2	13.1±3.7	12.0±4.2
Other ions	8.0±2.3	4.2±2.9	5.6±1.5	10.9±3.4	7.6±3.7
% of $PM_{2.5}$	62.7±4.9	43.2±7.4	49.3±8.5	52.6±7.3	52.1±9.7
TC	**16.0±3.3**	**12.1±1.6**	**21.0±11.8**	**22.3±8.6**	**19.2±9.3**
OC	11.2±2.6	7.9±0.8	13.2±7.8	18.3±8.1	13.8±7.5
EC	4.8±0.9	4.2±1.2	7.7±4.5	4.0±0.9	5.4±3.2
% of $PM_{2.5}$	15.0±2.5	15.0±6.5	20.3±8.2	17.6±3.3	17.8±6.1
OA	**18.9±4.1**	**14.0±1.4**	**21.6±11.9**	**31.2±11.9**	**23.3**±9.0
WSOA	14.1±3.0	12.1±2.4	15.6±6.6	25.1±8.6	18.1±6.1
WIOA	4.8±2.6	1.9±1.8	5.9±7.2	6.1±10.6	5.2±7.6
% of $PM_{2.5}$	17.8±3.2	18.2±8.4	20.9±8.3	24.6±6.3	21.5±6.8
PAHs ($ng\ m^{-3}$)	**41.42±24.7**			**140.25±60.2**	
Trace elements			**2.77±1.15**	**6.38±3.14**	
OA+EC+WSIIs	**90.2±21.0**	**53.2±21.6**	**83.1±29.6***	**108.4±36.3***	**85.1±27.9**
% of $PM_{2.5}$	**85.1±5.6**	**65.8±5.4**	**80.4±15.0***	**85.4±12.9***	**78.6±11.6**

*These values also include contributions from trace elements.

1056 Table 4. Mean concentration (ng m^{-3}) and mass fractions (%) of individual PAH to the total

1057 PAHs.

PAH compounds	Number of rings	Molecular formula and molecular weight (MW)	**Winter**		**Spring**	
			Conc. (ng m^{-3})	% of total	Conc. (ng m^{-3})	% of total
NaP	2-rings	$C_{10}H_8$,128	10.12	7.22	2.60	6.28
Acy		$C_{12}H_8$,152	0.16	0.12	0.08	0.20
Ace		$C_{12}H_{10}$,154	0.15	0.11	0.34	0.83
Flu	3-rings	$C_{13}H_{10}$,166	1.19	0.85	1.70	4.11
Phe		$C_{14}H_{10}$,178	3.54	2.52	3.24	7.83
Ant		$C_{14}H_{10}$,178	0.46	0.33	0.54	1.31
Flua		$C_{16}H_{10}$,202	8.05	5.74	2.57	6.21
Pyr		$C_{16}H_{10}$,202	8.93	6.37	2.43	5.87
BaA	4-rings	$C_{18}H_{12}$, 228	11.6	8.27	1.88	4.53
Chr		$C_{18}H_{12}$, 228	15.41	11.0	4.32	10.43
BbF+BjF		$C_{20}H_{12}$, 252	12.19	8.69	3.89	9.39
BkF		$C_{20}H_{12}$, 252	5.58	3.98	1.87	4.50
BaP	5-rings	$C_{20}H_{12}$, 252	10.33	7.37	3.43	8.29
BeP		$C_{20}H_{12}$, 252	12.08	8.61	2.42	5.83
DBA		$C_{22}H_{14}$, 278	2.53	1.8	0.42	1.02
InP	6-rings	$C_{22}H_{12}$, 276	20.74	14.8	5.23	12.62
BghiP		$C_{22}H_{12}$, 276	17.18	12.3	4.46	10.76
LMW-PAHs	2-3 rings		15.62	11.1	8.50	20.6
MMW-PAHs	4-rings		43.99	31.4	11.20	27.0
HMW-PAHs	5-6 rings		80.63	57.5	21.72	52.4
ΣPAHs			140.25	100.0	41.42	100.0

1058

Table 5. Cross-correlation coefficients (*r*) of the measured concentrations of the PAH species and ratios of the mean concentrations between these species from GC-MS (bold) and SP-AMS (italic).

PAHs	$C_{16}H_{10}$	$C_{18}H_{12}$	$C_{20}H_{12}$	$C_{22}H_{12}$	Ratio (GC)	Ratio (SP-AMS)
$C_{16}H_{10}$	1	*-0.250*	*-0.062*	*-0.140*	**$C_{16}H_{10}/C_{16}H_{10}$=1**	*$C_{16}H_{10}^{+}/C_{16}H_{10}^{+}$=1*
$C_{18}H_{12}$	**0.952**	**1**	*0.572*	*0.528*	**$C_{16}H_{10}/C_{18}H_{12}$=0.84**	*$C_{16}H_{10}^{+}/C_{18}H_{12}^{+}$=0.43*
$C_{20}H_{12}$	**0.936**	**0.994**	1	*0.771*	**$C_{16}H_{10}/C_{20}H_{12}$=0.36**	*$C_{16}H_{10}^{+}/C_{20}H_{12}^{+}$=0.56*
$C_{22}H_{12}$	**0.925**	**0.986**	**0.993**	1	**$C_{16}H_{10}/C_{22}H_{12}$=0.35**	*$C_{16}H_{10}^{+}/C_{22}H_{12}^{+}$=1.17*

$C_{16}H_{10}$: Flua+Pyr; $C_{18}H_{10}$: BaA+Chr; $C_{20}H_{12}$: BbF+BjF+BkF+BaP+BeP;
$C_{22}H_{12}$: BghiP+InP+DBA

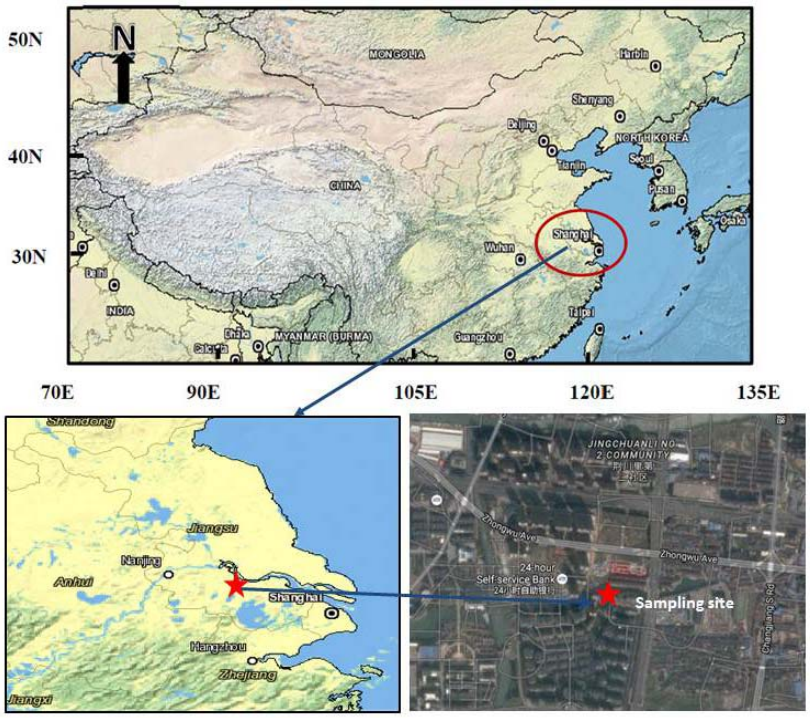

1065

1066 Figure 1. Schematic map of the sampling site and its surroundings.

1067

1068

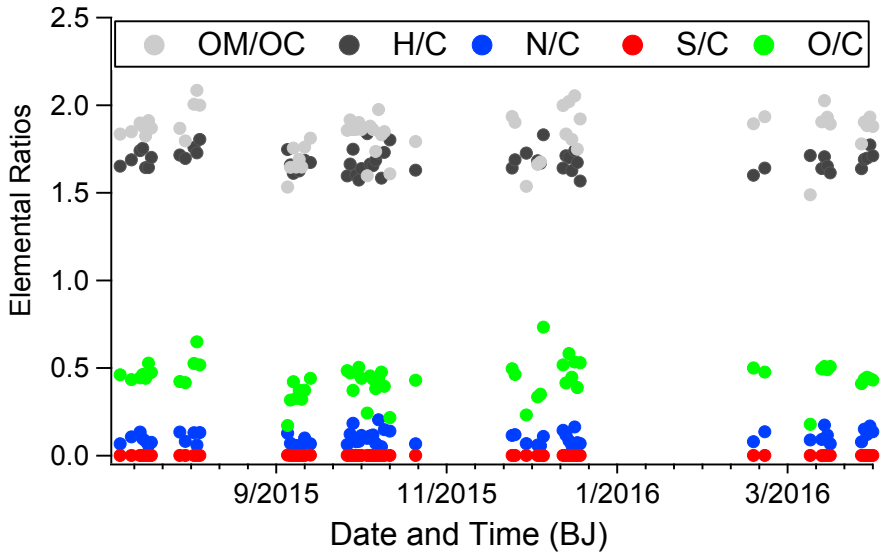

Figure 2. The atomic elemental ratios for the water-soluble organic aerosols (WSOA) determined by the SP-AMS.

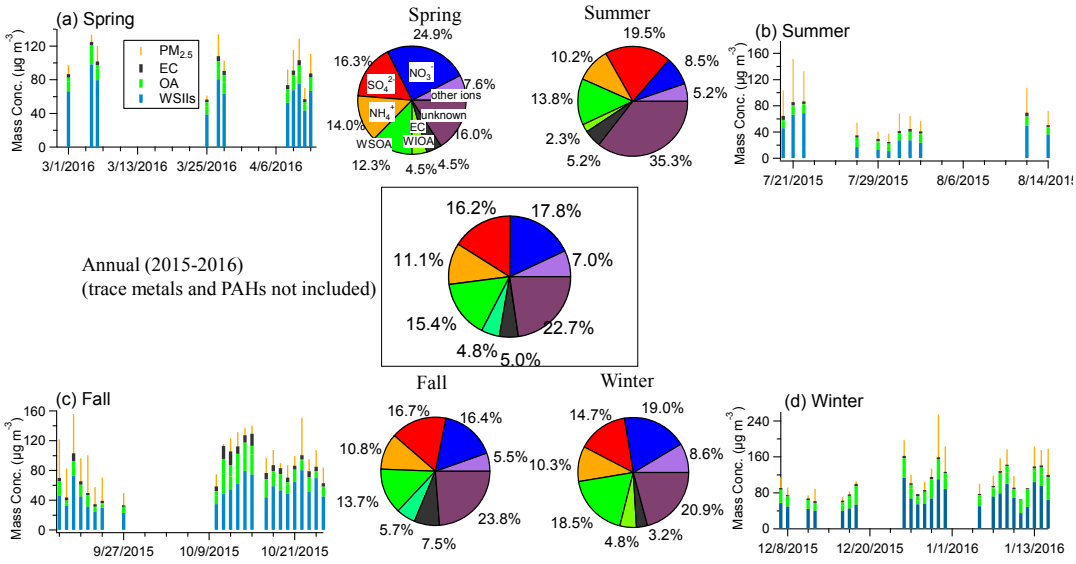

Figure 3. Reconstructed mass (= OA + EC + WSIIs) *vs.* $PM_{2.5}$ mass from gravimetric measurement in (a) spring, (b) summer, (c) fall, (d) winter, and annual. Corresponding pie charts show the mass percentages of different species to the $PM_{2.5}$ mass (trace elements and PAHs are not included due to sample limitations).

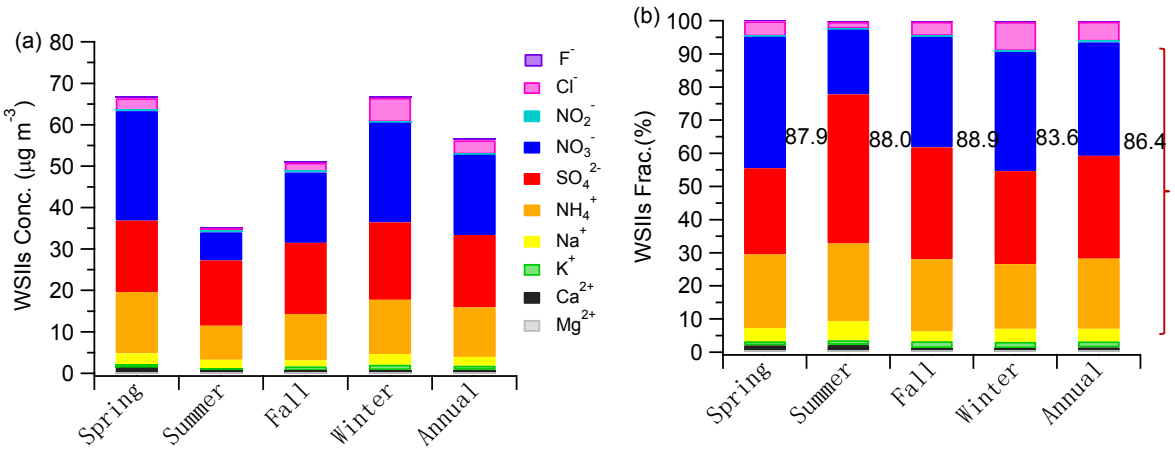

1083

1084

1085 Figure 4. (a) Seasonal variations of average mass concentrations and (b) mass fractional

1086 contributions of WSIIs in $PM_{2.5}$ in Changzhou during 2015-2016. The values marked in (b) are

1087 the fractions of three most abundant ions (NO_3^- + SO_4^{2-} + NH_4^+) to the total WSIIs.

1088

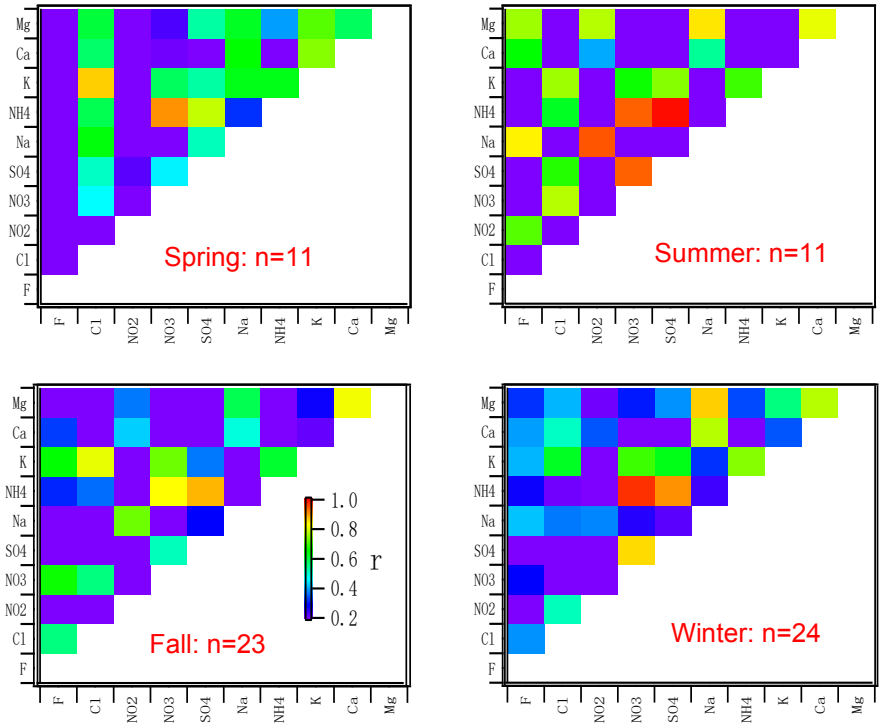

1089

1090 Figure 5. Image plots showing the cross correlation coefficients (*r*) between water-soluble ions

1091 in $PM_{2.5}$ in four seasons (colored by *r*).

1092

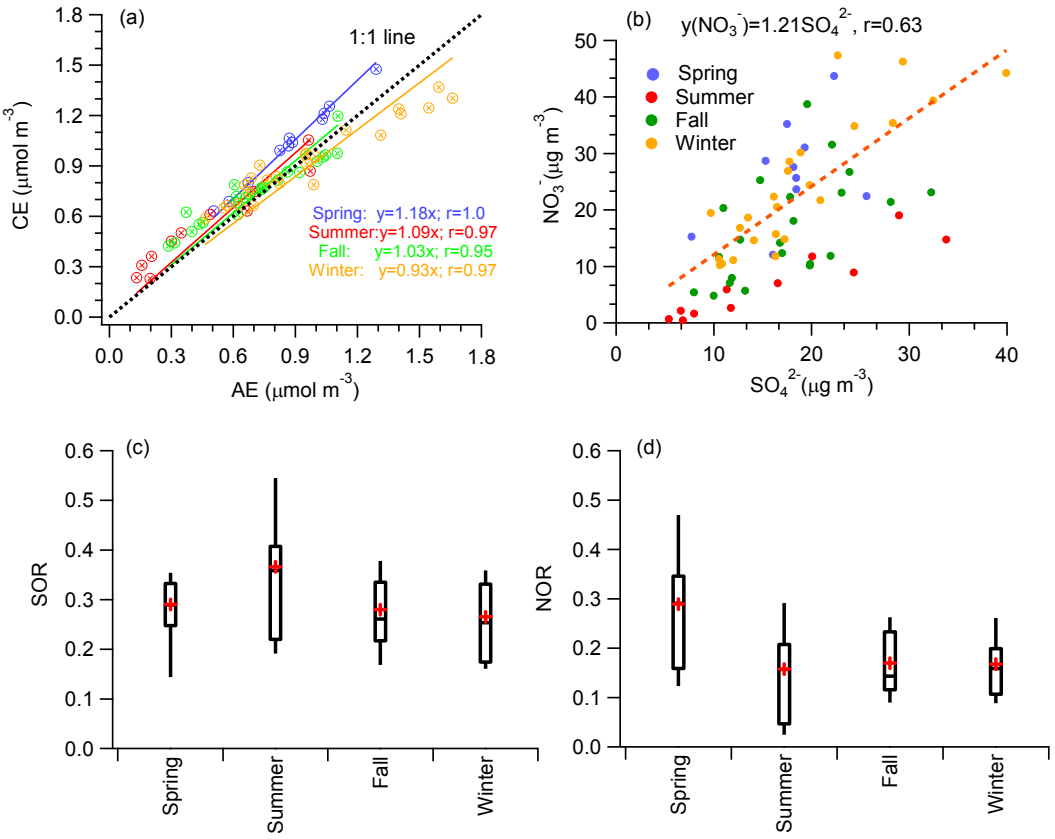

Figure 6. (a) Scatter plots of molar concentrations of cations *vs.* anions, (b) scatter plots of NO_3^- *vs.* SO_4^{2-} concentrations, (c-d) SOR and NOR value during four seasons. In (a), the dashed line refers to 1:1 line. In (b), the dashed line was the averaged fitted line, representing NO_3^-/SO_4^{2-} ratio during the entire period. Data in different seasons are shown by different colors for comparison. Linear regression equations were also presented. In (c-d), the crosses represent the mean, the middle bars represent the median, the top and bottom of the box represents the 75th and 25th percentile, respectively, and the top and bottom whiskers represent the 90th and 10th percentile, respectively.

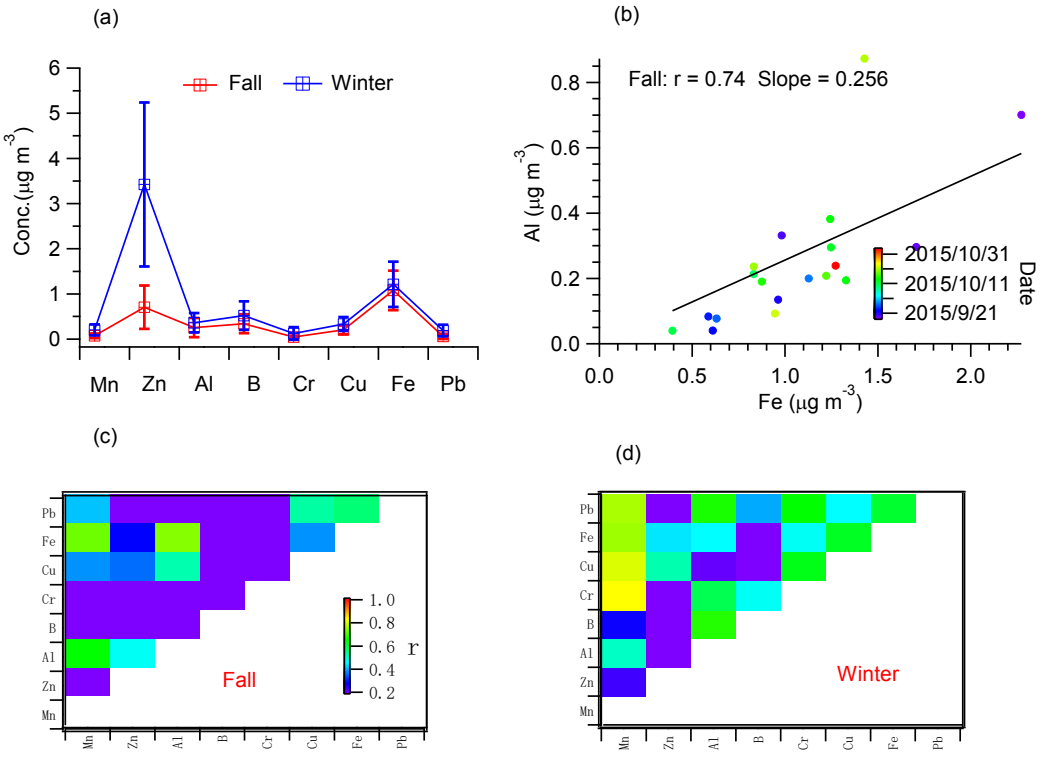

Figure 7. (a) Mean mass concentrations of trace elements determined for fall and winter (error bar represents the measurement uncertainty), (b) scatter plots of Al *vs.* Fe in fall, and (c-d) cross-correlation coefficients (*r*) among different trace elements in fall and winter, respectively (colored by *r*).

1110

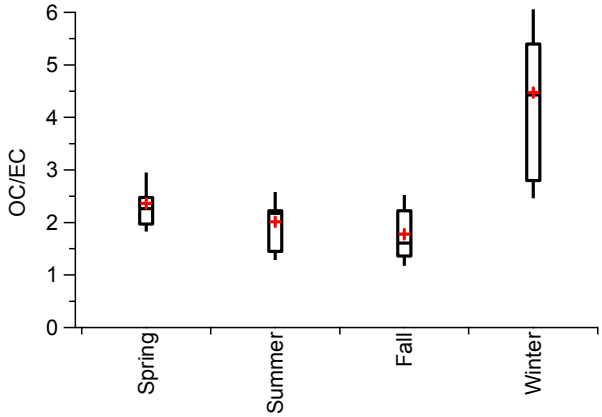

1111

1112 Figure 8. Average OC/EC ratios measured in four seasons (symbols of the box plots are the

1113 same as described in Figure 6.)

1114

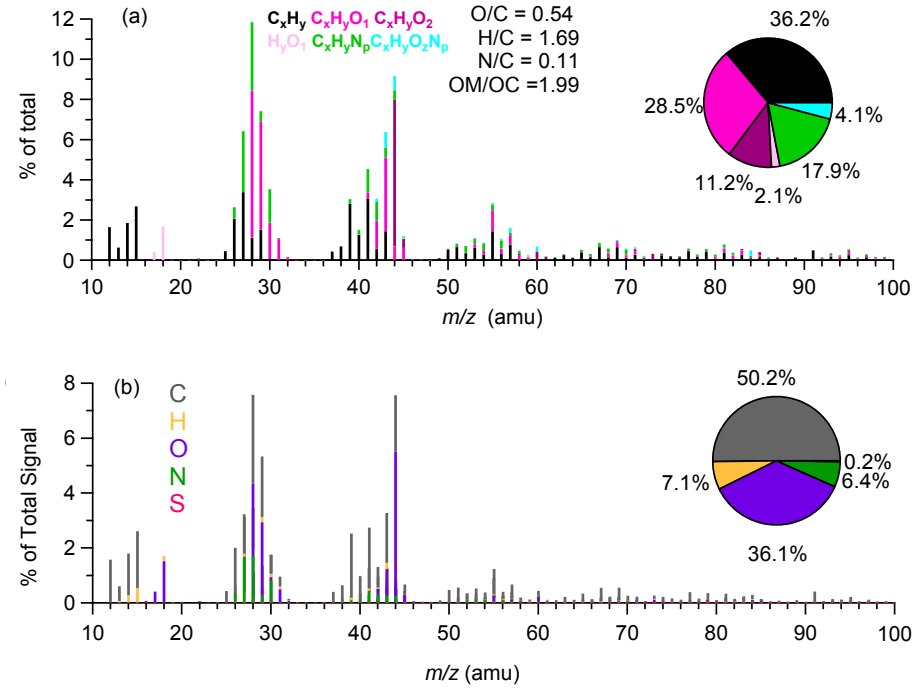

Figure 9. (a) High-resolution mass spectral profile of the WSOA measured by the SP-AMS (Mass spectrum is classified and colored by six ion families; pie chart shows the mass contributions of each ion family to the total MS), (b) Average mass spectrum classified by five elements (C, H, O, N, and S) (inset pie chart shows mass contributions of the five elements, respectively).

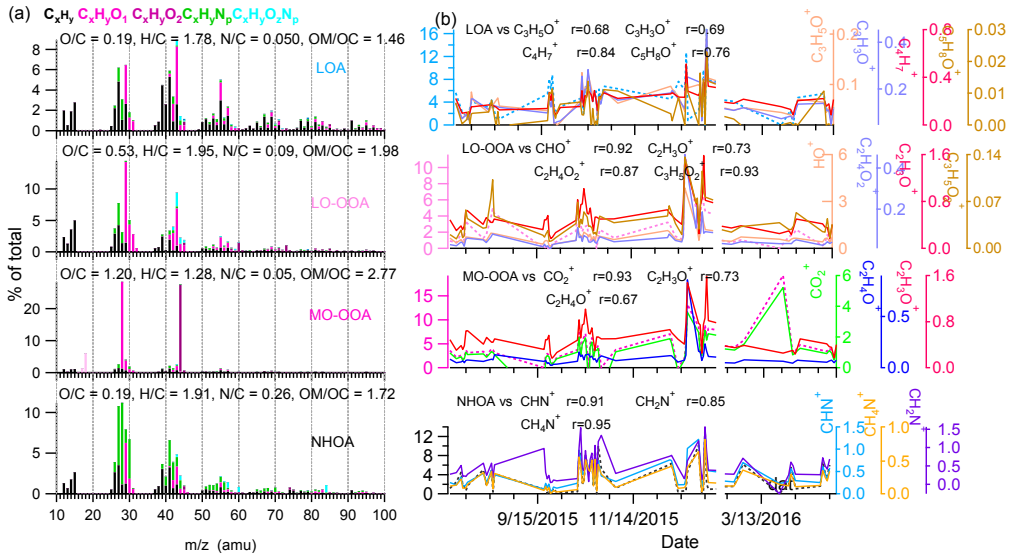

1122

1123 Figure 10. (a) High-resolution mass spectra of nitrogen-enriched hydrocarbon-like OA (NHOA),
1124 local primary OA (LOA), less-oxidized OA (LO-OOA) and more-oxidized OA (MO-OOA)
1125 separated by the PMF analyses, colored by six ion categories, (b) time series of the four WSOA
1126 factors, and corresponding tracer ions.

1127

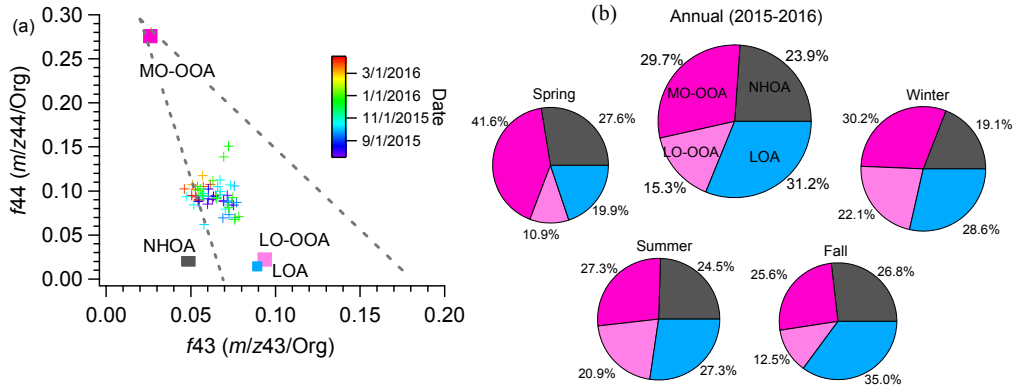

Figure 11. (a) Triangle plot of *f*44 *vs.* *f*43 for all WSOA, and the four WSOA factors identified by the PMF analyses, (b) pie charts of the mass contributions of four WSOA factors to the total WSOA in four seasons and the whole sampling period.

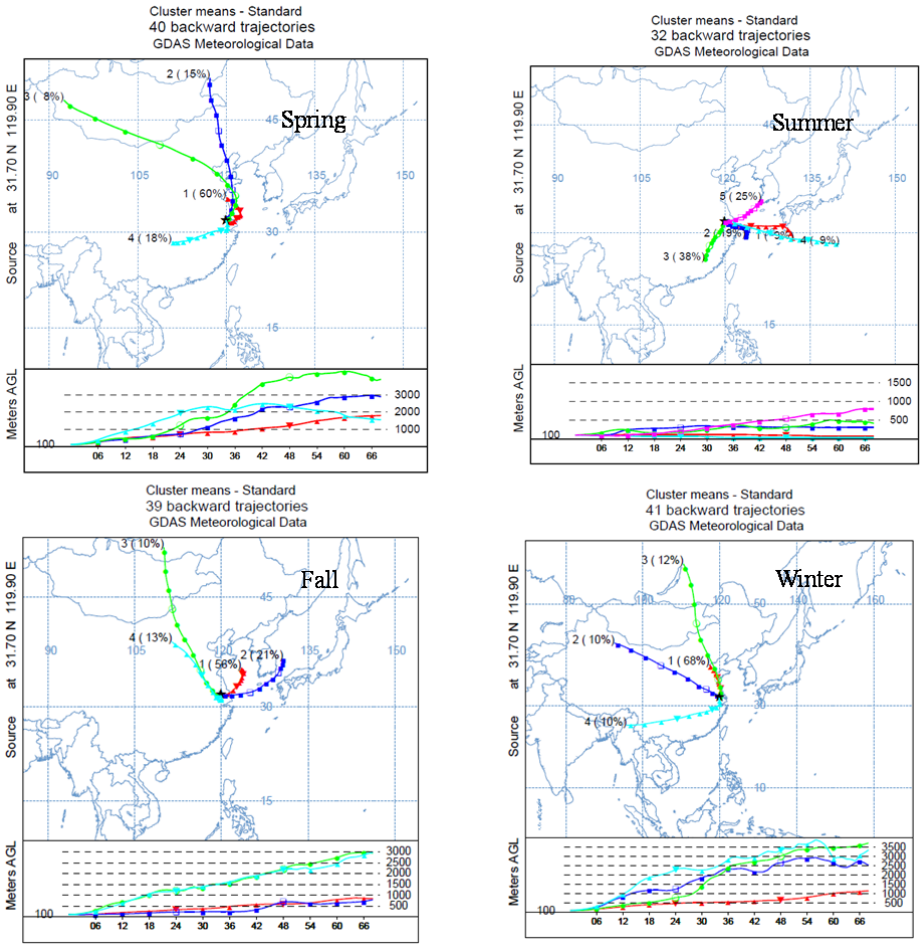

Figure 12. Air mass back trajectories across four seasons during the sampling period.